Susana dos Reis Gregório

Licenciatura em Bioquímica

Improvement of viral fusion inhibitor enfuvirtide efficacy by conjugation with membrane anchoring lipids

Dissertação para obtenção do Grau de Mestre em Bioquímica

Orientador: Prof. Doutor Nuno C. Santos, Professor Associado com Agregação, IMM, FMUL
Co-orientador: Doutor Axel Hollmann, Investigador Pós-Doc, IMM; Professor Instrutor, UNQ

Júri:

Presidente: Prof. Doutor José Ricardo Ramos Franco Tavares
Arguente: Prof. Doutor Pedro Miguel Ribeiro Viana Baptista
Vogal: Prof. Doutor Nuno Correia Santos

FACULDADE DE CIÊNCIAS E TECNOLOGIA
UNIVERSIDADE NOVA DE LISBOA

Novembro 2014

“Copyright”

Improvement of viral fusion inhibitor enfuvirtide efficacy by conjugation with membrane anchoring lipids

Susana dos Reis Gregório

Faculdade de Ciências e Tecnologia

Universidade Nova de Lisboa

Acknowledgements

Firstly, I would like to express my gratitude to Prof. Nuno C.Santos, my supervisor, for giving me the opportunity to develop my master thesis in his research group. I am grateful for the encouragement, support and all the scientific help throughout this work. I also would like to thank Dr. Axel Hollmann, my co-supervisor, for his help, support, comprehension and never-ending patient throughout this year. His guidance and motivation were essential for the completion of this thesis.

I would like to thank Dr. Sónia Gonçalves, Marcelo Augusto and Teresa Freitas for all their help in the experimental part.

To everyone from the Biochemistry Institute, especially to my colleagues of the Biomembranes Unit and Physical Biochemistry Unit, I would like to thank for the friendly environment.

I also would like to thank "Juniors" for the friendship, good moments and the so inspiring In&In conversations. Thank you for the great environment and for making it a fun place to work.
To Ana, my thesis partner, I would like to thank your support, fellowship, great conversations and especially your friendship. Without you this would not have been the same.

To all my friends, especially to Inês, Sara e Márcia, thank you for all the support and for being always there for me. I am grateful to be able to call you friends.

Last but not least, I would like to thank my parents, Adriano e Natália, and my sister Filipa for all the support, never-ending encouragement and for always believing in me, even when I didn't. Thank you for everything!

Resumo

O vírus da imunodeficiência humana tipo 1 (VIH-1) é um vírus altamente patogénico e evasivo para o qual ainda não foi desenvolvida uma cura. A maioria dos fármacos antirretrovirais desenvolvidos contra esta infeção tem como alvo enzimas chave do seu ciclo replicativo, como a transcriptase reversa, integrase e protease. Um processo crucial na infeção pelo VIH é a fusão das membranas viral e do hospedeiro, pelo que o desenvolvimento de uma nova classe de antirretrovirais, os inibidores de fusão, apresenta uma grande vantagem face aos fármacos comummente usados na terapêutica, uma vez que estes atuam antes da libertação do genoma viral nas células do hospedeiro. Em estudos anteriores foi reportado que a atividade antiviral de péptidos inibidores de VIH-1 é amplificada pela conjugação com colesterol e polietilenoglicol (PEG). Assim, o objetivo deste trabalho é a caracterização da interação de péptidos que derivam do enfuvirtide, pela conjugação com colesterol, ácido palmítico ou α-tocoferol como âncoras lipídicas e PEG como espaçador, com sistemas membranares modelo e células sanguíneas humanas.

Recorrendo a metodologias de espectroscopia de fluorescência, incluindo ensaios de partição e de extinção de fluorescência, demonstrou-se que a conjugação com porções lipídicas potencia a interação dos péptidos com membranas de diferentes composições lipídicas. Foi também averiguada a localização dos péptidos na membrana utilizando sondas lipofílicas, verificando-se que os péptidos conjugados se encontram numa posição mais superficial do que o não conjugado.

A avaliação de alterações do potencial de dipolo da membrana permitiu verificar que os péptidos conjugados apresentam uma maior afinidade para membranas ricas em colesterol, assim como para células sanguíneas, contrariamente ao péptido não conjugado.

De modo geral, os resultados obtidos indicam que um balanço entre a afinidade para a membrana e a exposição dos péptidos é essencial para o aumento da atividade antiviral dos mesmos. Assim, a adição de frações lipídicas a um inibidor de fusão reconhecido poderá ser uma estratégia promissora no combate à infeção por VIH-1.

Palavras-chave: VIH-1; Inibidor de fusão; Enfuvirtide; Lípidos de ancoragem membranar

Abstract

The human immunodeficiency virus type 1 (HIV-1) is a highly pathogenic and evasive virus, for which no cure has yet been achieved. The majority of the antiretroviral drugs developed over the years against this infection target key enzymes in HIV life cycle, such as reverse transcriptase, integrase and protease. Fusion of viral and host cell membranes is a crucial step in virus infectivity; therefore, the development of viral entry inhibitors has great advantages over conventional drugs, since they prevent the release of the viral content into the host cell. Previous studies showed that the antiviral activity of HIV-1 inhibitor peptides is increased by the addition of cholesterol and polyethylene glycol (PEG). The aim of the present work is to characterize the interaction of enfuvirtide derived molecules by conjugation with cholesterol, palmitic acid or α-tocopherol as lipid anchors and PEG as spacer, with biomembrane model systems and human blood cells.

Fluorescence spectroscopy methodologies, including membrane partition and fluorescence quenching assays, demonstrated that conjugation with lipids increases the peptides ability to interact with membranes of different compositions. In addition, the depth of peptide insertion into the membrane was assessed using lipophilic probes, revealing that the conjugated peptides are located in a more shallow position than the unconjugated one. Moreover, dipole potential assays showed that conjugated peptides exhibit a higher affinity towards cholesterol-rich membranes, as well as human blood cells, than the unconjugated peptide.

Altogether, the obtained results indicate that a proper balance between membrane affinity and peptide exposure is required in order to enhance antiviral activity. Therefore, the addition of lipid moieties to an established fusion inhibitor such as enfuvirtide can be a promising strategy against HIV-1.

Keywords: HIV-1; Fusion inhibitor; Enfuvirtide; Membrane anchoring lipids

Contents

Figures Index

Tables Index

Abbreviations and symbols

16NS	16-doxyl-stearic acid
5NS	5-doxyl-stearic acid
6HB	Six-helix bundle
Abs_F	Absorbance of the fluorophore at the initial concentration
Abs_T	Absorbance of the total solution
AIDS	Acquired immunodeficiency syndrome
ANS	8-anilino-1-naphthalenesulfonic acid (ammonium salt)
CCR5	C-C chemokine receptor type 5
CD4	Cluster of differentiation 4
CF	Correction factor
Chol	Cholesterol
CHR	C-terminal heptad repeat
CT	Cytoplasmic tail
CXCR4	C-X-C chemokine receptor type 4
di-8-ANEPPS	4-[2-[6-(dioctylamino)-2-naphthalenyl]ethenyl]-1-(3-sulfopropyl)-pyridinium
Env	Envelope glycoprotein
ER	Endoplasmic reticulum
FP	Fusion peptide
gp120	Envelope glycoprotein 120
gp160	Envelope glycoprotein 160
gp41	Envelope glycoprotein 41
HAART	Highly active antiretroviral therapy
HEPES	4-(2-hydroxyethyl)piperazine-1-ethanesulfonic acid
HIV	Human immunodeficiency virus
HIV-1	Human immunodeficiency virus type 1
HIV-2	Human immunodeficiency virus type 2
HR	Heptad repeat domain
IC_{50}	Half maximal inhibitory concentration
LBD	Lipid binding domain
LUV	Large unilamellar vesicles
MLV	Multilamellar vesicles
MPER	Membrane proximal external region

NHR	N-terminal heptad repeat
Palm	Palmitic acid
PBD	Pocket binding domain
PBMC	Peripheral blood mononuclear cells
PEG	Polyethylene glycol
POPC	1-palmitoyl-2-oleyl-*sn*-glycero-3-phosphocholine
RAFI	Rigid amphipathic fusion inhibitors
SEM	Standard error of mean
SIV	Simian immunodeficiency virus
SM	Sphingomyelin
TM	Transmembrane domain
Toco	α-tocopherol
TRD	Tryptophan-rich domain
Trp	L-tryptophan
UNAIDS	United Nations Programme on AIDS
VIRIP	Virus inhibitory peptide
WHO	World Health Organization

I	Fluorescence intensity
I_0	Fluorescence intensity at zero concentration of quencher
I_L	Fluorescence intensity in lipid
I_W	Fluorescence intensity in aqueous solution
K_d	Dissociation constant
K_p	Partition coefficient
K_{SV}	Stern-Volmer constant
L	Lipid
n_L	Number of moles of lipid
n_W	Number of moles of water
$n_{peptide,L}$	Number of moles of peptide present in the lipid phase
$n_{peptide,W}$	Number of moles of peptide in the aqueous phase
Q	Quencher
R	Intensities ratio
R_0	Intensities ratio in the absence of peptide
R_{min}	Asymptotic minimum value of the intensities ratio

R_{norm}	Intensities ratio normalized to the initial ratio
R	Correlation coefficient
V_L	Volume of the lipid phase
V_W	Volume of the aqueous phase
γ_L	Lipid molar volume
γ_W	Water molar volume
λ_{exc}	Excitation wavelength
$\Delta\Psi$	Transmembrane potential
Ψ_d	Dipole potential
Ψ_S	Surface potential

1. Introduction

1.1. HIV: origin and diversity

Human immunodeficiency virus (HIV) is the causative agent of the acquired immunodeficiency syndrome (AIDS), one of the most extreme cases of immune suppression caused by a pathogen (*Murphy*, 2011). Although the earliest documented case of HIV infection has been reported in samples of serum and lymph node biopsy from the present Democratic Republic of Congo, stored in 1959 and 1960, respectively (*Worobey et al.*, 2008; *Zhu et al.*, 1998), it was only in 1981 that AIDS was officially recognized; as an unusual pattern of symptoms observed in a small group of previously healthy homosexual men in USA (*Gottlieb et al.*, 1981). Soon after, AIDS cases were reported in other groups, including intravenous drug users and hemophiliacs (*Davis*, 1983; *Masur et al.*, 1981). HIV was identified and isolated for the first time in 1983 (*Barré-Sinoussi et al.*, 1983), being consider as the causative agent of AIDS (*Coffin et al.*, 1986).

Since the beginning of HIV epidemic, nearly 75 million people have been infected, with an outcome of about 36 million deaths. By the end of 2013, the United Nations Programme on AIDS (UNAIDS)/World Health Organization (WHO) epidemic update estimated 35.0 million (33.2 – 37.2 million) people were living with HIV, wherein 2.1 million (1.9 – 2.4 million) were newly infected people, and 1.5 million (1.4 – 1.7 million) died due to AIDS (*UNAIDS*, 2014).

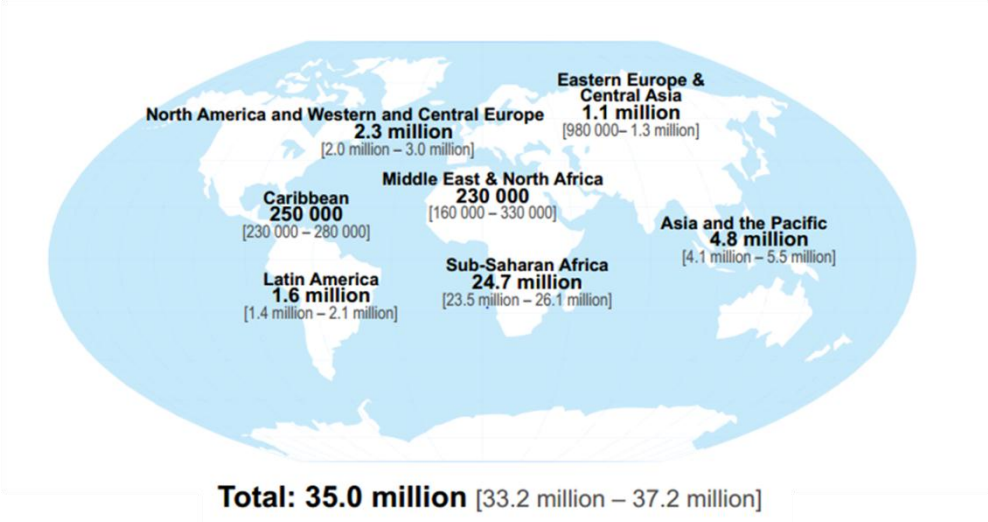

Figure 1.1 - Geographic distribution of adults and children estimated to be living with HIV in 2013.
Worldwide, 35.0 million people were living with HIV at the end of 2013 (*UNAIDS*, 2014).

Human immunodeficiency viruses belong to the *Lentivirus* genus, *Retrovididae* family and comprise two types of virus: HIV-1 and HIV-2. Although AIDS can be caused by both viruses, their origin and gene sequence differ. HIV-1 is the most virulent specie and progresses more rapidly to AIDS than HIV-2 (*Weiss*, 2000).

HIV and their lineages derived from multiple and independent zoonotic transmissions, *i.e.* cross-species transmissions, of simian immunodeficiency virus (SIV) from nonhuman primates into human in West and Central Africa; HIV-1 derived from the chimpanzee, *Pan troglodytes*, whereas HIV-2 from

the sooty mangabey, *Cercocebus atys.* HIV-2 is endemic in West Africa, however the virus' prevalence spread to Europe (especially Portugal) and India. The zoonotic transmissions by chimpanzees led to several HIV-1 lineages, groups M, N, O and P. Group M (Major/Main), which include various subtypes, is the most common and is responsible for the HIV-1 worldwide pandemic (*Hemelaar*, 2012; *Reeves & Doms*, 2002). A tremendous genetic variability, due to high mutations and recombinant rates of the reverse transcriptase enzyme which lacks a proof-reading mechanism, and high rates of virus replication are crucial factors in the worldwide spread of HIV, causing the virus to be highly adaptable to new hosts and selection pressures (*Hemelaar*, 2013).

1.2. HIV transmission and progression of disease

HIV infection takes place when body fluids are transferred from an infected person to an uninfected one. The virus can be transmitted through contaminated blood products (injection, blood transfusion/organ transplant), vertically (from mother to child) in pregnancy, birth or breastfeeding and, most frequently, through sexual activity (*Murphy*, 2011).

Unlike several other viruses, HIV infection rarely leads to an immune response that prevents the ongoing virus replication; however, HIV does not cause AIDS immediately (*Murphy*, 2011). In the acute infection phase, within 2-6 weeks after HIV exposure, up to 80% people develop flu-like symptoms. This primary infection is clinically characterized by an increased viremia and a pronounced decrease in circulating $CD4^+$ T cells, which are destroyed by the virus itself after replication, or by apoptosis. After this period, $CD8^+$ T cells (a cytotoxic T cell that kills HIV-infected cells) are activated and the number of $CD4^+$ cells begins to increase. The production of antibodies also takes place and their number rise to detectable levels whilst antigen levels becomes undetectable – seroconversion (*Murphy*, 2011). Besides the absence of symptoms, in the asymptomatic phase or clinical latency, the replication of the virus remains and the number of $CD4^+$ cells decreases gradually. In untreated patients, this period has an average duration of 10 years. After this period, the illness progresses to AIDS, increasing the susceptibility to infection with opportunistic pathogens and the occurrence of tumors that usually do not affect people with a healthy immune system. Figure 1.2 summarizes the disease progression of untreated HIV infection.

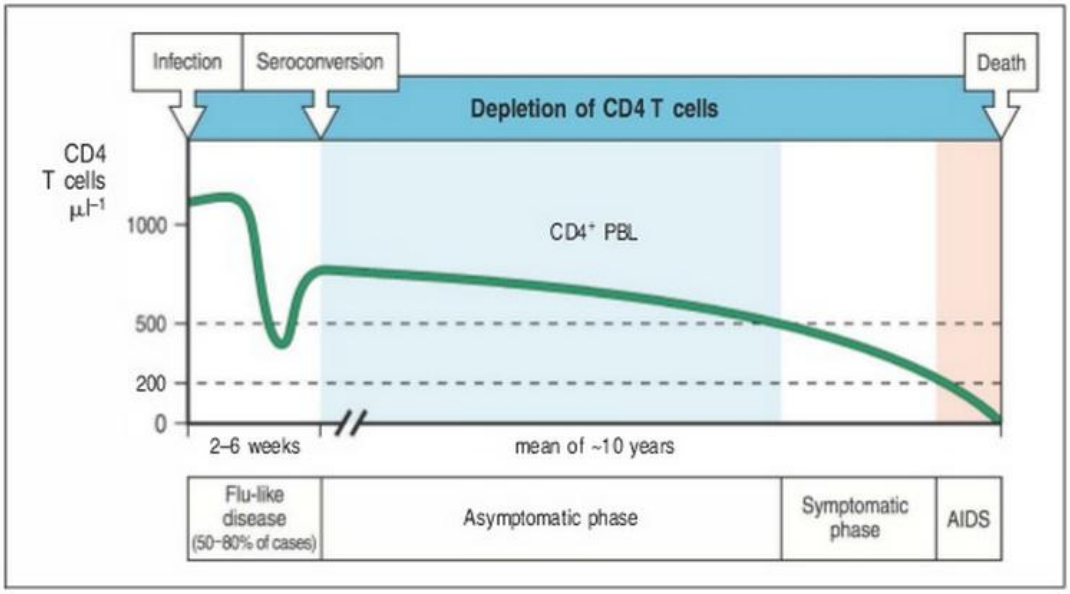

Figure 1.2 - The typical profile of untreated infection with HIV.
The acute phase occurs 2–6 weeks after infection and is marked by high levels of virus in the bloodstream. In the asymptomatic phase, an adaptive immune response follows the acute phase, controlling it and restoring $CD4^+$ T cells levels; however, without the complete removal of the virus. The symptomatic phase occurs as the $CD4^+$ T cells count falls to 500 cells.μL^{-1}, when opportunistic infections become more frequent. At a count of $CD4^+$ T cells bellow 200 cells.μL^{-1} the patient is said to have AIDS (*Murphy*, 2011).

1.3. HIV-1 structure and life cycle

HIV-1 is an enveloped virus that infects $CD4^+$ T cells, dendritic cells and macrophages (*Murphy*, 2011). HIV virions are spherical particles with ≈ 100 nm in diameter (*Sougrat et al.*, 2007), coated by a viral envelope membrane derived from the host cell plasma membrane, which covers and protects their capsid structures and the single-strand RNA copies (Figure 1.3). HIV-1 envelope glycoprotein (gene designation *Env*), whose function is to mediate binding and fusion of the viral membrane with the host cell membrane, is the only membrane protein encoded by the genomic RNA (*Blumenthal et al.*, 2012; *Podbilewicz*, 2014). Env is first synthesized in the endoplasmic reticulum (ER) as a precursor protein termed gp160. After glycosylation in the Golgi apparatus, the protein is cleaved by the cellular protease furin into two subunits: a surface subunit (gp120) and a transmembrane subunit (gp41) (*Hallenberger et al.*, 1992) that remain noncovalently associated, comprising a trimer of heterodimers. These glycoproteins are the main targets of HIV-1 neutralizing antibodies that, through selection, developed many mechanisms to evade the host immune response, making them the most variable proteins of HIV-1 (*Burton et al.*, 2004; *Wyatt*, 1998).

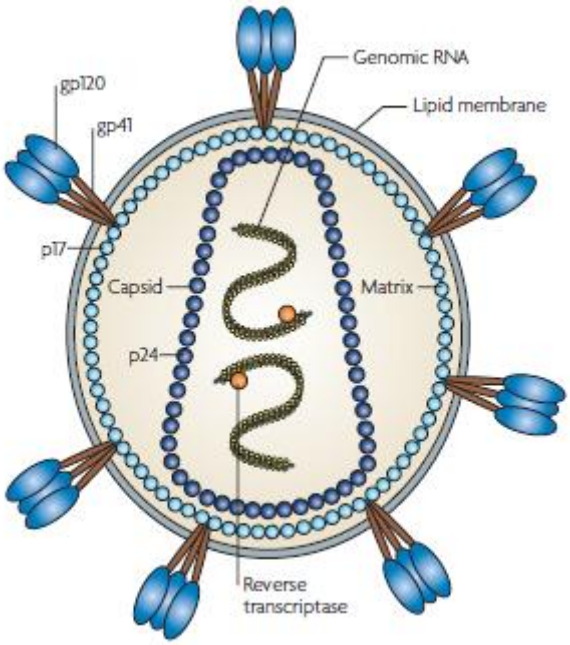

Figure 1.3 - Schematic representation of HIV-1 virion.
The trimeric gp120-gp41 complexes are embedded in the membrane. The cytoplasmic tail of gp41 interacts with p17, a viral protein that composes the matrix and surrounds the capsid. The capsid protein, p24, is organized into a cone shape ensuring the integrity of the viral genome. Two single-stranded RNA copies are surrounded by nucleocapsid proteins (in yellow) and enzymes essential to the development of the virion. Adapted from (*Karlsson Hedestam et al.*, 2008).

Each gp120 subunit contains an inner domain with five highly conserved regions, which are crucial to virus-cell attachment, and an outer domain with surface-exposed hypervariable loops (Figure 1.4), which are involved in immune evasion as they are a constantly moving target for the host's immune system (*Wilen et al.*, 2012).

An ectodomain (extracellular domain), a transmembrane domain (TM) and an endodomain (intracellular domain) compose each gp41 subunit. The latter, also referred as, cytoplasmic tail (CT) plays a role in packaging, infectivity and cell pathogenicity (*Yang et al.*, 2010). The transmembrane domain is responsible for Env's anchorage in the viral membrane (*Wilen et al.*, 2012). The ectodomain has a hydrophobic fusion peptide (FP) located at the N-terminal, whose function is to insert into the host membrane, and two heptad repeat regions, closer to the N-terminal (NHR) or C-terminal (CHR) (*Franquelim et al.*, 2011). A Trp-rich domain, the membrane proximal external region (MPER), where several antibodies bind, is located at the C-terminal, between the TM and the CHR, and also seems to play an important role during membrane fusion (*Lorizate et al.*, 2008).

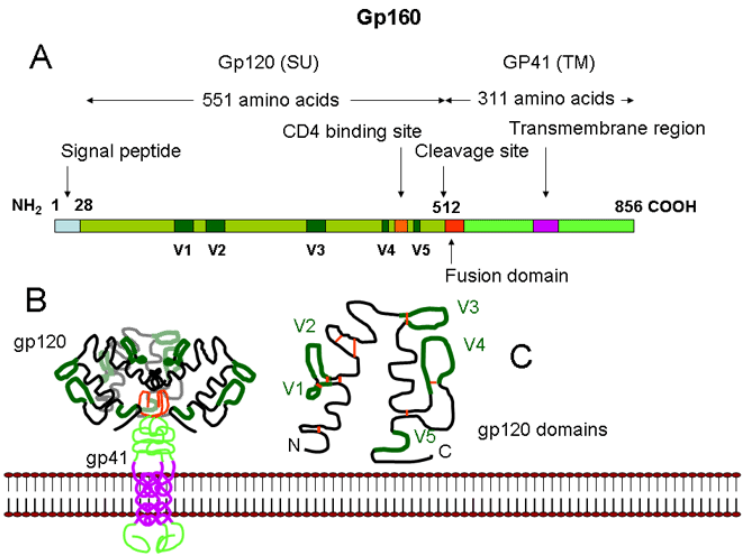

Figure 1.4 - Structure of gp160.
Gp160 comprises gp120 and gp41 (A). The homotrimer of gp120/gp41 heterodimers is associated with the viral membrane through the transmembrane region of gp41 (B). Gp120 has surface-exposed hypervariable loops (C). Red bars represent disulfide bridges. (Source: http://pathmicro.med.sc.edu/lecture/hiv9.htm)

Moreover, the genetic material of the virus is composed by two single-stranded RNA molecules surrounded by nucleocapsid proteins and enzymes that are required for the development of the virion, such as reverse transcriptase, protease and integrase, which are also in contact with HIV's genome. This structure is enclosed in a cone-shaped capsid comprised by the viral protein p24. To ensure the integrity of the virion, the capsid is surrounded by a matrix of viral proteins (*Karlsson Hedestam et al.*, 2008).

The HIV-1 replication cycle (Figure 1.5) can be divided into two phases, an early phase and a late one (*Tözsér*, 2003). The early phase begins with the attachment of the mature virion to the host cell membrane, leading to viral-cell membrane fusion, and entry of the cone-shaped capsid. At this stage, the viral RNA is released and, by reverse transcription, a double-stranded viral DNA is generated, which is then integrated into the host genome. In the late stage of the cycle, the viral DNA is transcribed into mRNA that encodes different viral proteins. At the end of this phase, the assembly of virion proteins and viral RNA takes place in the plasma membrane, and finally the immature virus exits the cell by a budding process followed by a protease-mediated maturation.

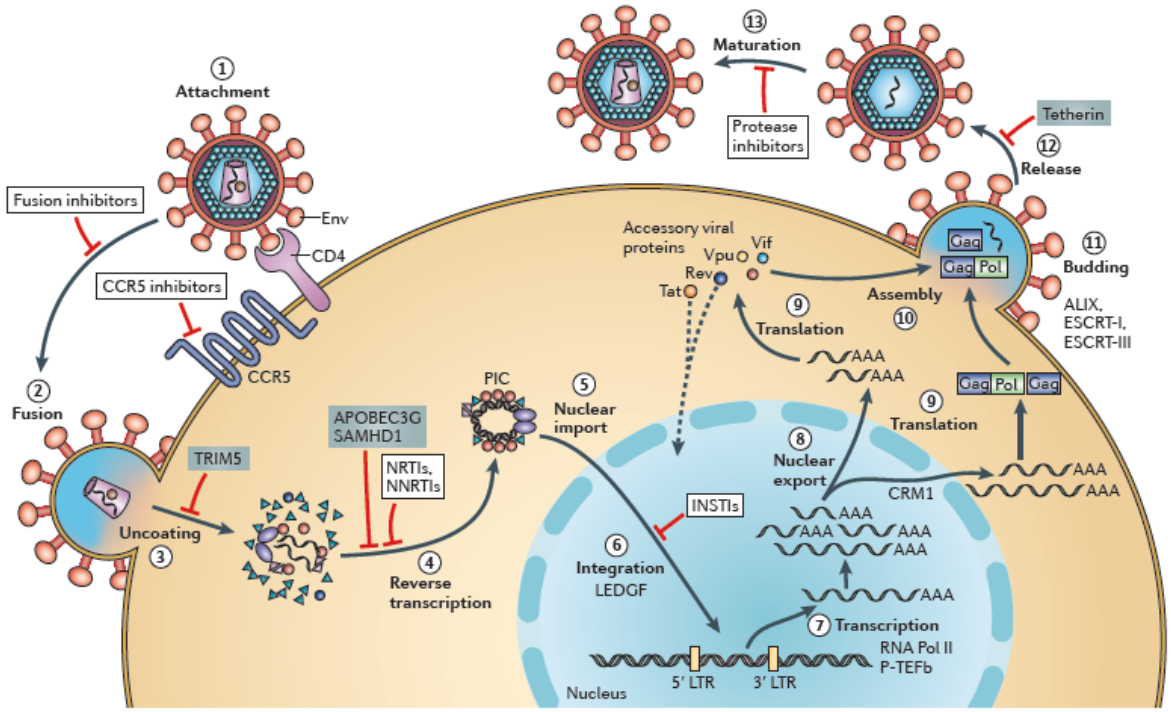

Figure 1.5 - Schematic representation of the HIV-1 cycle.
The infection begins with the attachment (1) to the host cell, followed by viral-cell membrane fusion (2). The uncoating and release of the viral genome (3) facilitates reverse transcription (4). The pre-integration complex (PIC) is transported to the cell nucleus (5) and the viral genome is integrated into the host genome (6). The proviral transcription (7) generates mRNAs of different sizes that are exported (8) from the nucleus and serve as templates for protein production (9).The viral components are assembled (10) and, by a budding process (11), the immature virion is released (12). At this stage, the virion undergoes a protease-mediated maturation (13) (*Engelman & Cherepanov*, 2012).

The research of HIV has been useful, not only for the understanding the nature of the disease, but also for prevention, diagnosis and treatment. Since HIV's discovery as the causative agent of AIDS, the development of anti-HIV drugs has been the focus of intense research (*De Clercq*, 2013). As a consequence, many drugs are now available, but still no cure or vaccine was achieved. The majority of the approved antiretroviral drugs target three essential enzymes of the HIV life cycle: reverse transcriptase, integrase and protease (*De Clercq*, 2009). As reviewed by *Adamson & Freed* (2010), these drugs have significantly extended the life-expectancy of HIV patients. The combination of several antiretroviral drugs, known as highly active antiretroviral therapy (HAART), is considered the standard treatment for HIV patients. Despite having the advantage of combining multiple drugs, preventing HIV's resistance to a single inhibitor, drug resistance can still emerge. As a consequence of this multi-drug resistance an alternative treatment, known as salvage therapy, is required. This will be more effective if new drugs are available.

Even though HIV infections decreased by 38% since 2001 and the treatment cost is more affordable, and consequently a higher number of people are receiving HIV treatment, there are 22 million people to whom antiretroviral therapy is still inaccessible (*UNAIDS*, 2014). Therefore, the development of more potent and economically viable drugs is required.

1.3.1. HIV-1 entry and its inhibition

As an enveloped virus, HIV-1 must transfer its genetic material across both the viral and host membranes to infect a cell (*Doms & Trono*, 2000). The attachment and viral fusion with host's cell membrane are crucial steps in the HIV life cycle. The efficient blocking of these steps prevents the occurrence of the subsequent intracellular stages of the viral life cycle (*Hollmann et al.*, 2013).

HIV-1 entry into the host cell is a multi-step process that comprises attachment of the virus to the cell surface, receptor binding, co-receptor binding and membrane fusion (*Tilton & Doms*, 2010).

The first step of HIV-1 entry is the binding of gp120 to the CD4 receptor of the host cells (Figure 1.6). Gp120 has high affinity towards the cell-surface receptor: nevertheless, this event is not sufficient to trigger membrane fusion (*Klasse*, 2012; *Wilen et al.*, 2012). Therefore, gp120 must also bind to a co-receptor in host's membrane. There are two chemokine receptors that act as major co-receptors for viral entry, CCR5 and CXCR4, which use depends on the viral strain (*Locher et al.*, 2005). The interaction of gp120 with the CD4 receptor causes conformational changes enabling the glycoprotein to bind to the co-receptor. At this stage, the hydrophobic N-terminal gp41 fusion peptide is exposed and interacts with the membrane of the host cell, into which it inserts, prompted by a tripled-stranded coiled-coil (*Doms & Trono*, 2000), formed by the NHR from each gp41 of the trimer. During membrane fusion both helical domains of the gp41, NHR and CHR, folds into each other in an antiparallel fashion, resulting in a highly stable structure named six-helix bundle (6HB). The 6HB structure brings the viral and cell membranes into close proximity, allowing membrane fusion and, consequently, the release of the viral content into the host cell (*Wilen et al.*, 2012).

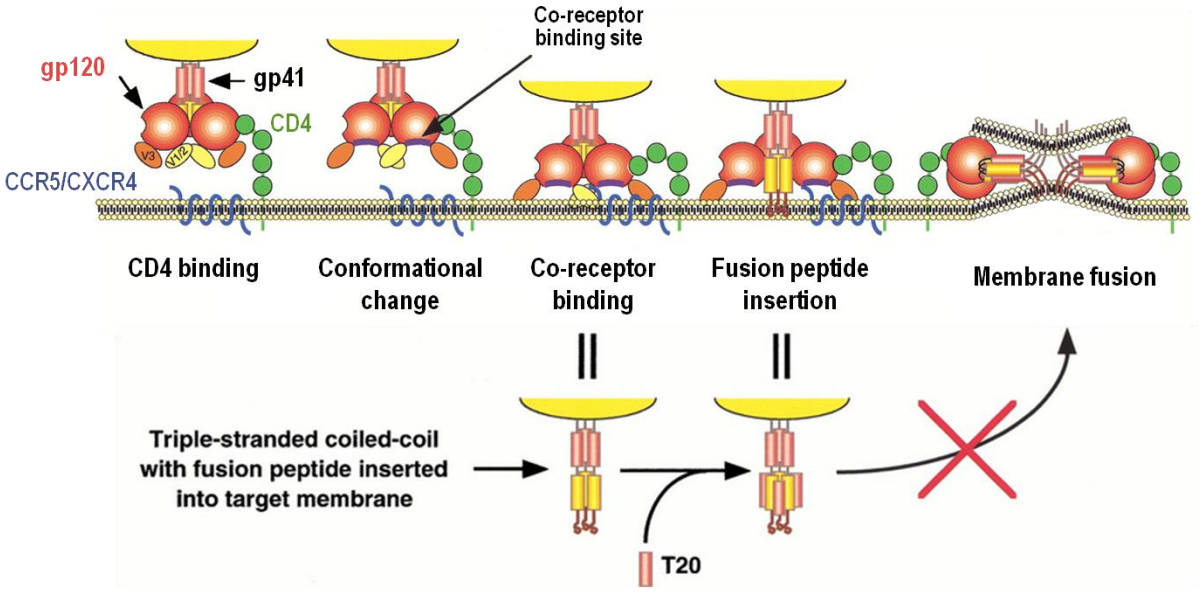

Figure 1.6 - Entry mechanism of HIV-1.
The viral envelope gp120 binds to CD4 receptor, inducing conformational changes that promote co-receptor binding. This engagement results in the exposure of the gp41 fusion peptide and its insertion into the target membrane. The formation of a hairpin-like structure, in which gp41 folds back on itself, brings the viral and cell membranes into close proximity and membrane fusion occurs. The bottom part of the figure displays gp41 alone; addition of the T20 peptide blocks membrane fusion (*vd. infra*). Adapted from (*Doms & Trono*, 2000).

Despite HAART's efficiency at inhibiting HIV replication, reducing AIDS morbidity and mortality, it does not eradicate HIV infection (*Tilton & Doms*, 2010); patients require treatment indefinitely. As a result, long-term toxicity, drug-drug interactions and emergence of drug-resistance strains of HIV may arise, limiting treatment effectiveness. As a consequence, and also due to high costs of HAART, new strategies to inhibit viral replication have been investigated.

Since HIV-1 entry is a multi-step process involving multiple interactions between Env and host proteins, each step of the process can be a target for entry inhibitors. This new class of antiretroviral can be divided into three categories: attachment and CD4 inhibitors, co-receptor inhibitors and fusion inhibitors (*Wilen et al.*, 2012). Attachment inhibitors target the gp120-CD4 binding step by blocking the interaction between gp120 and the CD4 receptor, while antagonists of the co-receptors act on the binding step of gp120 to the co-receptor (CCR5 or CXCR4). Fusion inhibitors act on the gp41-mediated membrane fusion step (reviewed by Henrich & Kuritzkes 2013; Haqqani & Tilton 2013; Berkhout et al. 2012).

Despite this promising approach in drug development against HIV-1, until now, only two entry inhibitors were approved by the USA Food and Drug Administration (FDA), and are currently clinically available; maraviroc, an inhibitor of the gp120 binding to the CCR5 co-receptor (*Lieberman-Blum et al.*, 2008), and enfuvirtide (T20), a fusion inhibitor peptide that targets gp41 in its pre-hairpin conformation (*Matthews et al.*, 2004).

1.4. Fusion inhibitors

The initial development of HIV-1 fusion inhibitors was based on the heptad repeat domains (HR) of gp41 (*Jiang et al.*, 1993; *Wild et al.*, 1992). The formation of the 6HB by the back-folding of gp41 NHR and CHR is a critical step for membrane fusion; after pore formation in its pre-bundle complex, this structure also stabilizes and expands the nascent fusion pore (*Markosyan et al.*, 2003). Hence, the first strategy to suppress HIV-1 fusion was the use of synthetic peptides mimicking one of those domains. Peptides that mimic the NHR and CHR domains are known as N-peptides and C-peptides, respectively. These fusion inhibitors interact with gp41 domains interfering with the formation of the 6HB, and preventing the expansion and stabilization of the fusion pore (*Wilen et al.*, 2012).

Fusion inhibitors can be divided into different classes according to their interaction with gp41 (Figure 1.7). Class I fusion inhibitors are synthetic peptides that mimic the CHR domain of gp41 and act by competitively binding to NHR, thus preventing 6HB formation. C-peptides, such as enfuvirtide, T-1249, sifuvirtide and C34 belong to this class. Classes II and III include peptides that mimic the gp41 NHR domain, the N-peptides. These act by targeting the CHR region (class II) or by interspersing with the NHR region, preventing the trimerization of the NHR subunits (class III). Although peptides in these classes exhibit inhibitory activity against HIV, they are less potent than C-peptides, mainly due to their tendency to aggregate and low solubility, since N-peptides are rather hydrophobic (*Berkhout et al.*, 2012; *Franquelim et al.*, 2011). Class IV comprises monoclonal antibodies that target the membrane

proximal region of gp41 (*Reardon et al.*, 2014). Finally, class V includes peptides that target the gp41 fusion peptide, preventing its insertion into the target membrane and subsequent membrane fusion. To this class belongs a natural antiviral peptide present in human blood, termed virus inhibitory peptide (VIRIP) (*Münch et al.*, 2007).

Additionally, new classes of fusion inhibitors that target the viral membrane were also reported: rigid amphipathic fusion inhibitors (RAFI) (*St Vincent et al.*, 2010; *Vigant et al.*, 2013), small lipophilic molecules such as LJ001 or JL103 (*Vigant et al.*, 2013, 2014), or modified sterols as 25HC (*Liu et al.*, 2013). All these small molecules have the ability to modify biophysical properties of the membrane, preventing the fusion process.

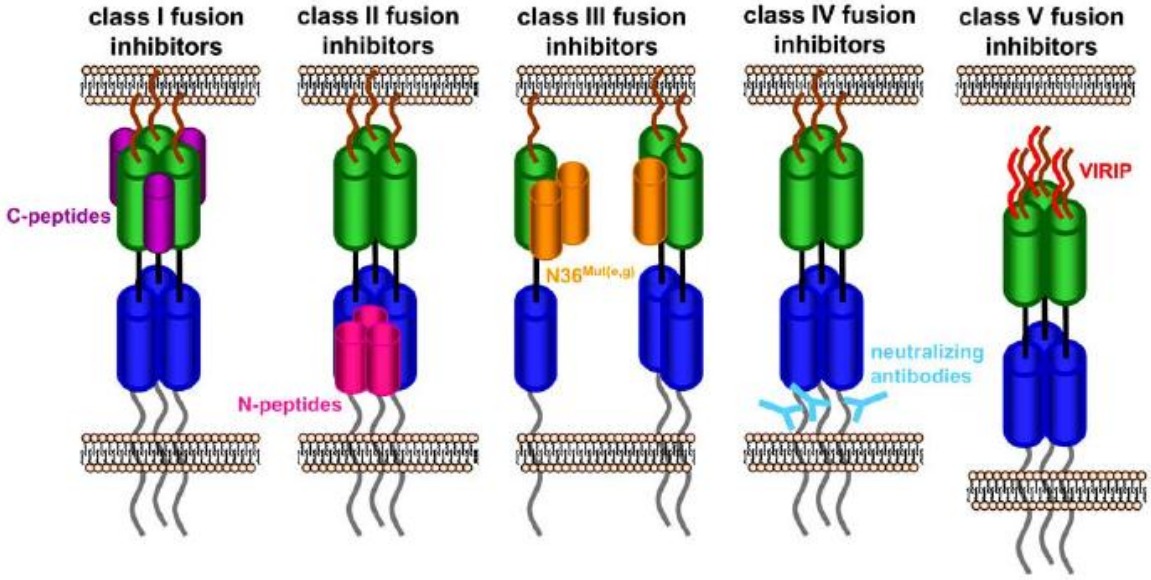

Figure 1.7 - Classes of HIV-1 fusion inhibitors.
Class I inhibitors mimic the gp41 CHR domain and bind to the NHR domain. Class II inhibitors mimic the NHR domain and bind to CHR. Class III inhibitors mimic the gp41 NHR domain, preventing the trimerization of NHR. In these three classes, the formation of the 6HB is prevented. Class IV inhibitors comprise antibodies that target the membrane proximal region, and in class V are comprised inhibitors that target the N-terminal fusion peptide of NHR. Adapted from (*Steffen & Pöhlmann*, 2010).

1.5. C-peptides: new strategies against HIV-1 fusion

Structural analysis of the trimeric gp41 structure and understanding the CHR and NHR interaction enabled the development of peptides derived from the gp41 sequence towards HIV inhibition (*Franquelim et al.*, 2011). The CHR region contains a pocket binding domain (PBD) complementary to deep hydrophobic pockets of the NHR core. Moreover, a HR core and a lipid binding domain (LBD) or tryptophan-rich domain (TRD) are also part of the CHR region.

C34, a C-peptide with 34 amino acids, was used to determine the trimeric coiled-coil structure of gp41 (*Chan et al.*, 1997). Despite its high antiviral activity *in vitro*, C34 is not a good drug candidate due to its low solubility (*Otaka et al.*, 2002) and other factors (some of them not totally understood), leading to low *in vivo* efficacy.

Enfuvirtide (T20) is a synthetic polypeptide of 36 amino acids that is homologous to the CHR domain of gp41. The interaction between enfuvirtide and the virus is still not completely clear and is fairly complex. Some authors proposed that the mechanism of action by which enfuvirtide inhibits viral fusion is different from the one accepted for C34; enfuvirtide may target multiple sites in gp41 and gp120 (*Liu et al.*, 2005, 2007; *Veiga et al.*, 2004a). Still, currently the most accepted mechanism for enfuvirtide is the one described for C-peptides in general (*Franquelim et al.*, 2011). As a class I fusion peptide, enfuvirtide engages in a coil-coil interaction with the gp41 NHR domain, thus blocking the 6HB formation and membrane fusion (*Matthews et al.*, 2004). However, enfuvirtide lacks the PBD region (Figure 1.8), important for high antiviral activity (*Chan et al.*, 1998). There are other drawbacks to enfuvirtide: due to its peptide nature, it has a poor bioavailability (has to be administered subcutaneously) and is more sensitive to degradation while in circulation, its short half-life (≈ 4 h) requires more frequent injections that can cause injection site reactions for patients, rapid emergence of resistant strains, and high costs of production. This makes the long-term use of enfuvirtide problematic. For these reasons, enfuvirtide is primarily used in salvage therapy in patients where previous antiretroviral treatment has failed. Nevertheless enfuvirtide has many advantages: it has a potent antiviral effect *in vitro* and *in vivo,* low toxicity as it targets the protein of the virus instead of host cells, and it is effective against multi-drug resistant strains (*Berkhout et al.*, 2012; *De Clercq*, 2009; *Greenberg & Cammack*, 2004; *Matthews et al.*, 2004).

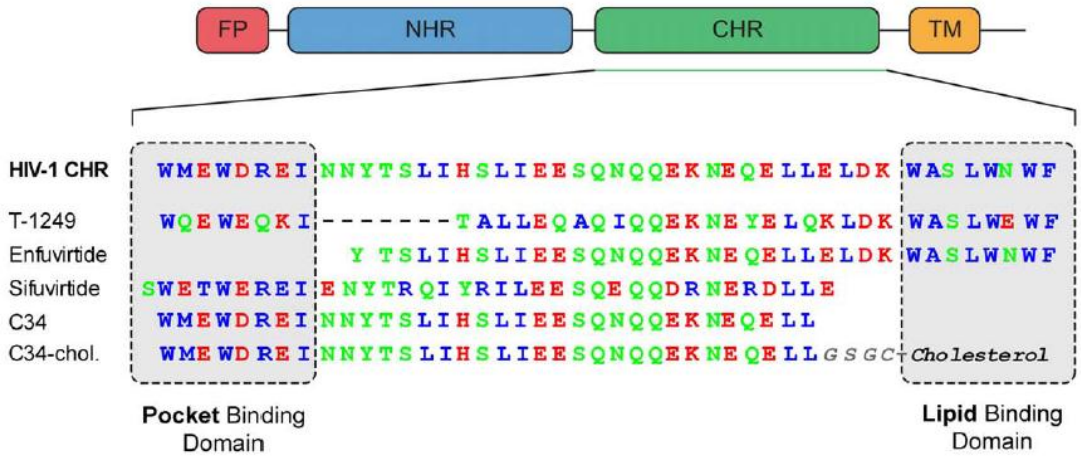

Figure 1.8 - Characteristics of several C-peptides.
Schematic representation of HIV-1 gp41 main domains; the relative position of the fusion peptide (FP), N-terminal heptad repeat domain (NHR), C-terminal heptad repeat domain (CHR) and transmembrane region (TM) are depicted. Several sequences of C-peptides were aligned, showing the pocket binding domain (PBD) and the lipid binding domain (LBP). Hydrophobic residues are represented in blue, non-charged polar residues in green, and charged polar residues in red. Adapted from (*Hollmann et al.*, 2013).

Based on the structural and functional information provided by C34 and enfuvirtide, new fusion peptides were developed.

T-1249 is a second generation fusion inhibitor. This peptide has 39 amino acid residues and was designed based on HIV-1, HIV-2 and SIV sequences (*Eron et al.*, 2004). Even though T-1249 presented higher antiviral activity and a longer half-life than enfuvirtide, clinical development of this peptide was suspended due to problems in drug formulation (*Martin-Carbonero*, 2004).

Three-dimensional structural information of HIV-1 gp41 allowed the development of another second-generation fusion inhibitor, sifuvirtide. It is a 36 amino acid peptide engineered with different sequence and/or location in relation to C34, enfuvirtide and T-1249. In phase Ia clinical studies, sifuvirtide showed a higher potency and half-life in humans compared to enfuvirtide, enabling less clinical dosage and frequency of injections. Moreover, it showed to be highly effective against enfuvirtide-resistant strains (*He et al.*, 2008b). Sifuvirtide successfully completed Phase IIb clinical trials (http://fusogen.com/en/company-news/177). Although sifuvirtide appear to be a good candidate towards HIV-1 inhibition, there is a continuous search to optimize fusion inhibitor peptides.

In 2001, a different approach was taken to overcome the drawbacks of enfuvirtide (*Hildinger et al.*, 2001), by expressing a membrane-anchored version of enfuvirtide on a T-cell helper line. It was shown that this modified peptide (a construct of enfuvirtide, a short linker and a transmembrane domain) exhibited more antiviral activity than the construct without the transmembrane domain. Additionally, mutations in the membrane-proximal region of enfuvirtide inactivated the free peptide, but did not have the same effect on the membrane-anchored version of enfuvirtide. These results suggest that binding the drug to the cell membrane has a positive effect on its efficiency.

Based on this approach, a modified fusion peptide was developed to improve the antiviral activity of C34 by the addition of a cholesterol (Chol) moiety to its C-terminal (*Ingallinella et al.*, 2009). It was

hypothesized that using a cholesterol group as lipid anchor would be the most suitable approach due to the role of lipid rafts in HIV infection. Lipid rafts are microdomains within the lipid membrane, enriched in cholesterol and sphingolipids, where several transmembrane proteins and receptors are concentrated, including CD4, the main receptor for HIV infection (*Aloia et al.*, 1988; *Brügger et al.*, 2006). Besides the high antiviral activity observed for C34-Chol, this peptide also presents an increased half-life *in vivo* (≈ 24 h) (*Ingallinella et al.*, 2009). Moreover, due to its cholesterol moiety, C34-Chol is able to partition into lipid membranes, especially cholesterol-rich domains (*Hollmann et al.*, 2013). The increased antiviral activity and improved pharmacokinetic properties, along with peptide accumulation at the site of action (*Augusto et al.*, 2014; *Hollmann et al.*, 2013; *Ingallinella et al.*, 2009), make this approach a good strategy for the development of new drugs.

While lipid conjugation is a preferential approach to improve peptide pharmacokinetics (*Madsen et al.*, 2007), the covalent attachment of a polyethylene glycol (PEG) polymer to proteins is the most well-established strategy to prolong the half-life of a drug (*Jevsevar et al.*, 2010).

1.6. Objectives in the context of the state-of-art

Despite major progresses in the development of new antiviral drugs, enfuvirtide still remains as the only class I fusion inhibitor peptide approved for the treatment of HIV by the USA Food and Drug Administration (FDA) and European Medicines Agency (EMA). In this context, and considering the advantage of the lesson of C34 peptide derivatization with PEG and cholesterol moieties, a new set of modified fusion inhibitors was designed: T20* (T20 or enfuvirtide with the additional GSGSGC residues on its C-terminal) was conjugated with different lipid moieties, namely cholesterol, palmitic acid (Palm) and α-tocopherol (Toco) as membrane anchors and a four residues PEG spacer in between the lipid and the peptide. As a result of this approach, 5 peptide derivatives were successfully synthetized and are the main focus of this work. The antiviral activity of these novel peptides showed higher antiviral activity than its parental T20*, being in this way promising candidates towards HIV inhibition.

As previously pointed out, the interaction of the inhibitor peptides with membranes is a key factor in the characterization and unravelling of the mechanism of action of these fusion inhibitors. Taking this into consideration, the aim of this work was to evaluate the interaction of this family of enfuvirtide-derived molecules with biomembrane model systems and human blood cells.

Fluorescence spectroscopy methodologies were used to achieve these objectives, by the determination of the partition coefficient of the peptides to membranes with different compositions. A fluorescent probe, di-8-ANNEPS, was also used to evaluate peptides' interaction with model membranes and human blood cells (erythrocytes and lymphocytes). Finally, in order to elucidate the in-depth location of the different peptides in the membrane, quenching assays using aqueous (acrylamide) and lipophilic (5NS and 16NS) quenchers were performed.

2. Materials and methods

2.1. Materials

T20* (M_W = 4997.4 g/mol), T20*-Chol (M_W = 5368.0 g/mol), T20*-PEG_4-Chol (M_W = 5615.3 g/mol), T20*-PEG_4-Palm (M_W = 5440.1 g/mol), T20*-Toco (M_W = 5412.0 g/mol) and T20*-PEG_4-Toco (M_W = 5659.3 g/mol) peptides were obtained on the context of a collaboration project with Prof. Matteo Porotto (Departments of Pediatrics and of Microbiology and Immunology, Weill Medical College of Cornell University, New York, USA).

Human blood samples were obtained from healthy volunteer donors at Instituto Português do Sangue (IPS), Lisbon, under an institutional agreement between IPS and Instituto de Bioquímica from Faculdade de Medicina da Universidade de Lisboa, with their informed written consent. The samples were drawn to K_3EDTA anticoagulant tubes (Vacuette, Greiner Bio-One, Kremsmünster, Austria) and processed shortly after. This study was approved by the joint Ethics Committee of Faculdade de Medicina da Universidade de Lisboa and Hospital de Santa Maria (Lisbon).

POPC (1-palmitoyl-2-oleyl-*sn*-glycero-3-phosphocholine) and SM (egg sphingomyelin) were purchased from Avanti Polar Lipids (Alabaster, AL, USA). Acrylamide and HEPES (4-(2-hydroxyethyl)piperazine-1-ethanesulfonic acid) were obtained from Fluka (Buchs, Switzerland). $KHCO_3$ (potassium hydrogencarbonate), EDTA (ethylenediaminetetraacetic acid), cholesterol, Pluronic-F127, ANS (8-anilino-1-naphthalenesulfonic acid ammonium salt), 5NS (5-doxyl-stearic acid) and 16NS (16-doxyl-stearic acid) were acquired from Sigma-Aldrich (St. Louis, MO, USA). The fluorescent probe di-8-ANEPPS (4-[2-[6-(dioctylamino)-2-naphthalenyl]ethenyl]-1-(3-sulfopropyl)-pyridinium) was purchased from Invitrogen - Molecular Probes (Eugene, OR, USA). Lymphoprep™ was obtained from Stemcell Technologies (Vancouver, BC, Canada). Chloroform, DMSO (dimethyl sulfoxide), methanol, NaCl (sodium chloride), NH_4Cl (ammonium chloride) and L-Tryptophan were acquired from Merck (Darmstadt, Germany).

HEPES buffer (HEPES 10mM pH 7.4 in NaCl 150 mM) was the working buffer used throughout the experiments. L-Tryptophan 500 µM stock solution was prepared in buffer, while ANS 2 mM and acrylamide 4 M solutions were prepared in ultrapure H_2O. Stock solutions of the fluorescent probe di-8-ANEPPS 1 mg/mL and the lipophilic quenchers 5NS and 16NS 70 mM were prepared in ethanol. All stock solutions were stored at 4 ºC, except 5NS and 16NS (stored at -20 ºC).

2.2. Methods

2.2.1. Peptides

The peptides used in this work derive from enfuvirtide (T20), which amino acid sequence is YTSLIHSLIEESQNQQEKNEQELLELDKWASLWNWF. T20* and its derivatives have the same amino acid sequence, followed by 6 additional amino acid residues (GSGSGC), added before a lipid moiety -

cholesterol (Chol), palmitic acid (Palm) or α-tocopherol (Toco) - with or without a four unit polyethylene glycol (PEG) spacer in between, as presented in Figure 2.1.

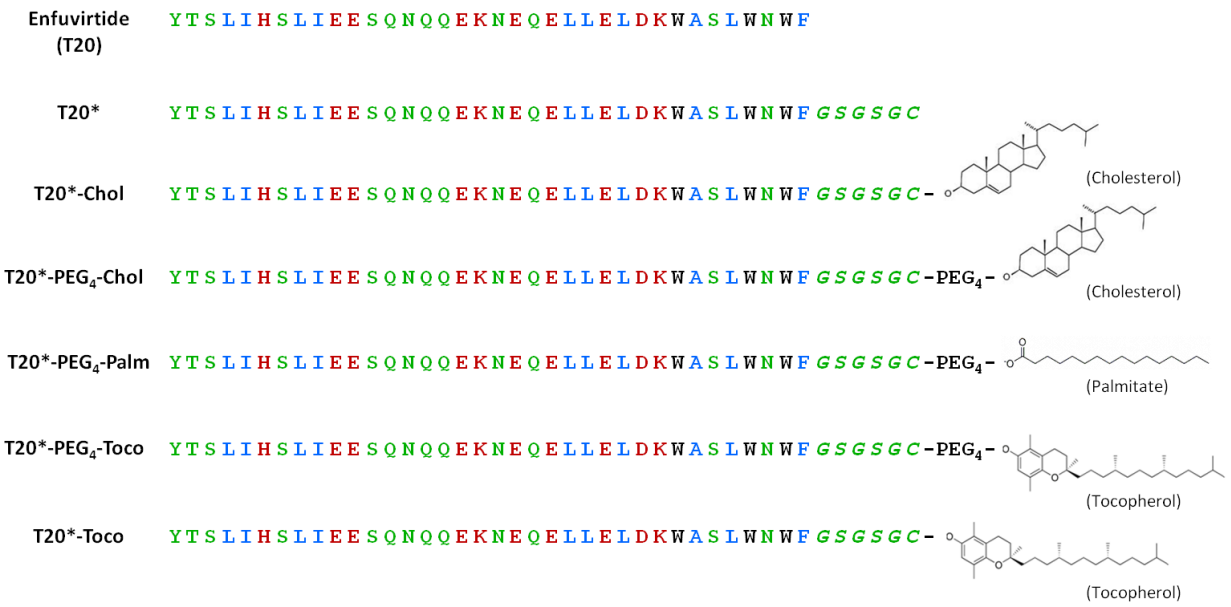

Figure 2.1 - Representation of enfuvirtide, T20* and its lipid derivatives.
Non-charged polar residues are represented in green, charged polar residues in red and hydrophobic residues in blue, wherein the three tryptophan residues (W) are shown in black.

Stock solutions of each peptide, with a final concentration of 500 μM, were prepared in dimethyl sulfoxide (DMSO) and stored at 4 ºC.

2.2.2. Biomembrane systems preparation

Liposomes

Different lipids such as POPC, Chol and SM were weighed to generate vesicles of diverse compositions: pure POPC, POPC:Chol (2:1) and POPC:Chol:SM (1:1:1). The lipids were dissolved in an organic solvent (POPC and POPC:Chol in chloroform and POPC:Chol:SM in a chloroform:methanol (12:1) mixture), and mixed in a round-bottom flask. A thin lipid film was formed by solvent evaporation using a gentle N_2 (g) flow. In order to remove residual organic solvent and, therefore, obtain a completely dried film, the flask was connected to a vacuum pump overnight. The dried lipid film was hydrated with buffer (HEPES) and, at least, 8 freeze-thaw cycles were performed until the formation of a liposome suspension of multilamellar vesicles (MLV). Large unilamellar vesicles (LUV) were obtained by extrusion (*Mayer et al.*, 1986), using a mini-extruder (Avanti Polar Lipids, Alabaster, AL, USA), 1001RN syringes (Hamilton, Reno, NV, USA) and 100 nm pore polycarbonate 10 mm diameter membranes (Nucleopore-Whatman, Kent, UK). LUV with, approximately, 100 nm of diameter were obtained.

Biological samples

Erythrocytes isolation

Blood samples were centrifuged for 10 min at 1200 *g* (Sorvall TC6 Centrifuge, H400 rotor) to remove plasma and buffy-coat. Isolated erythrocytes were washed, at least twice with working buffer, and a 100% hematocrit sample was obtained (*Matos et al.*, 2010a).

Peripheral blood mononuclear cells (PBMC) isolation

PBMC were isolated from blood samples using a density gradient medium Lymphoprep^{TM}. Samples were centrifuged for 30 min at 540 *g*, allowing the removal of plasma, isolation of buffy-coat containing the desired cells and keeping the erythrocytes' pellet intact (*Matos et al.*, 2010a). Isolated PBMC were washed at least twice with working buffer and an erythrocytes lysis buffer (157 mM NH_4Cl, 10 mM $KHCO_3$, EDTA 5%, pH 7.4) was used in order to prevent possible contaminations. In the washing steps, samples were centrifuged for 10 min at 100 *g*.

2.2.3. Fluorescence spectroscopy measurements

Peptide aggregation

T20* derivatives, by being conjugated with lipid moieties, are prone to aggregation when in aqueous solutions; hence, protein aggregation was monitored by ANS fluorescence. ANS is an amphiphilic fluorescent probe sensitive to its microenvironment and is commonly used to evaluate the presence of hydrophobic pockets in proteins and peptides. The probe exhibits a low quantum yield (and therefore, low fluorescence emission) in aqueous solution; however, when located in a less polar environment, its quantum yield (and fluorescence intensity) increases, and its emission maximum shifts to lower wavelengths (*Henriques et al.*, 2008).

A solution containing 12.8 μM of ANS in HEPES buffer was titrated with a stock solution of each peptide to achieve a final concentration within the 0-8 μM range. ANS fluorescence emission spectra were obtained from 400 to 600 nm, with an excitation wavelength (λ_{exc}) of 369 nm, using an Edinburgh Instruments FLS920 Series fluorescence spectrophotometer (Livingston, UK). Excitation and emission bandwidths were set to 5 and 10 nm, respectively.

Partition coefficient determination

Fluorescence spectroscopy is a valuable and sensitive tool to assess the partition coefficient of a molecule. An alteration on a fluorescence property of a membrane probe or a difference in a fluorescence parameter such as quantum yield, fluorescence anisotropy or fluorescence lifetime of the partitioning molecule upon incorporation in the membrane, enables the determination of the partition coefficient.

The intrinsic fluorescence of T20* and its conjugates, as these peptides contain three tryptophan residues, allows the quantification of its membrane insertion. The fluorescence of this aromatic amino acid is strongly dependent of the physical properties of its micro-environment and can change significantly upon peptides' insertion in the membrane.

For each peptide, the partition coefficient between an aqueous and a lipid phase in equilibrium can be described as (*Matos et al.*, 2010b; *Santos*, 2003):

$$K_p{}' = \frac{\frac{n_{peptide,L}}{n_L + n_{peptide,L}}}{\frac{n_{peptide,W}}{n_W + n_{peptide,W}}} \tag{2.1}$$

where n_L and n_W are the moles of lipid and water and $n_{peptide,L}$ and $n_{peptide,W}$ are the moles of peptide in lipid and water, respectively. Under most experimental conditions, the quantity of peptide is considerably lower in both phases than the total quantities of water or lipid ($n_{peptide,i} \ll n_i$), therefore this equation can by simplified to:

$$K_p{}' \approx \frac{\frac{n_{peptide,L}}{n_L}}{\frac{n_{peptide,W}}{n_W}} \tag{2.2}$$

In most literature it is common to represent the partition coefficient as a function of the volumes of each phase (V_i) instead of the water and lipid quantities:

$$K_p = \frac{\frac{n_{peptide,L}}{V_L}}{\frac{n_{peptide,W}}{V_W}} \tag{2.3}$$

This parameter, named the Nernst partition coefficient can be related with equation (2.2) by:

$$K_p = K_p{}' \frac{\gamma_W}{\gamma_L} \tag{2.4}$$

where γ_i is the molar volume of water ($i = W$) or lipid ($i = L$).

As mentioned before, the fluorescence intensity, I, can be measured as long as a peptide fluorescence parameter, such as the quantum yield, has a significant difference in the aqueous environment and the lipid membrane, and its partition coefficient can be determined measuring the tryptophan fluorescence intensity with a fixed concentration of peptide and an increasing lipid concentration ([L]). These measurements usually give rise to a hyperbolic I vs. [L] variation profile that can be fitted using:

$$I = \frac{I_W + K_p \gamma_L [L] I_L}{1 + K_p \gamma_L [L]} \quad (2.5)$$

Diverse membrane compositions, specifically POPC, POPC:Chol (2:1) and POPC:Chol:SM (1:1:1), were used to assess the peptides' membrane partition coefficient. A fixed concentration of 10 μM of peptide in a HEPES buffer solution was titrated with a 15 mM LUV suspension, freshly prepared, yielding a final lipid concentration ranging from 0 to 5 mM. Preceding the fluorescence emission analysis, an incubation time of 10 min was used after each addition of LUV suspension, to stabilize peptides' interaction with lipid membranes. The fluorescence emission spectrum of each peptide was recorded between 310 and 450 nm, considering that the maximum emission of the tryptophan residue in aqueous solution is 350 nm, and a λ_{exc} of 280 nm was used. The lipid titration was also performed on samples without peptide. Samples containing HEPES buffer and a tryptophan solution (30 μM) in HEPES buffer, both with DMSO as well, were used as a blank and control, respectively.

The intensity data of the nonpartitioning Trp was used to correct the scattering effects resulting from the successive addition of LUV. The correction factor for each addition is as follows (*Ladokhin et al.*, 2000):

$$I_{peptide}^{corrected}([L]) = I_{peptide}([L]) \frac{I_{Trp}^{buffer}}{I_{Trp}[(L)]} \quad (2.6)$$

where $I_{peptide}$ is the fluorescence intensity of the peptide, $[L]$ the lipid concentration and I_{Trp}^{buffer} and I_{Trp} the fluorescence intensity of the tryptophan residue in the absence and presence of the lipid, respectively.

Membrane dipole potential assessment

Cellular lipid bilayers have three types of electrostatic potentials associated to them: transmembrane potential, $\Delta\Psi$, as a result of an imbalance of charge and an electrical potential difference across the membrane by the selective transport of ions and, therefore, a difference in the ion concentration in both sides of the membrane; surface potential, Ψ_S, generated by the charged head-groups of phospholipids and the adsorbed ions at the interface, resulting in an accumulation of charges in the outer surface of the membrane; and dipole potential, Ψ_d, which arises from the orientation of dipole residues of lipids (polar head-groups and glycerol-ester regions) and water molecules hydrating the surface of the membrane (*Matos et al.*, 2008; *Wang*, 2012).

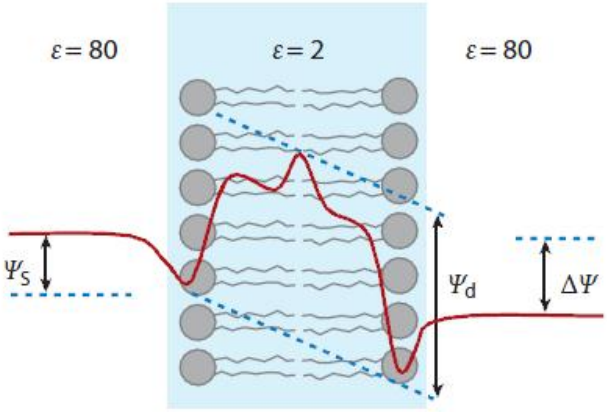

Figure 2.2 - Schematic representation of the three types of membrane potential.
$\Delta\Psi$ is the transmembrane potential, Ψ_S, the surface potential and Ψ_d is the dipole potential. Typical values of dielectric constant, ε, are given (*Wang*, 2012).

Since the dipole potential originates from oriented dipoles in the membrane/water interface, macromolecules interacting with lipid membranes can cause a change in the potential by the destabilization of such organization and/or by the contribution of their own dipoles to the membrane dipole potential. Thus, monitoring dipole potential alterations is a useful tool to study membrane interactions with molecules, such as proteins and peptides, particularly if they are not intrinsically fluorescent. Moreover, this avoids the requirement to derivatize peptides and proteins, which can modify their structure and, consequently, the function of these molecules. This strategy is also advantageous on the study of cell systems, as the peptides' intrinsic fluorescence is interfered by other cellular proteic components (*Matos et al.*, 2010b; *Wang*, 2012). Regardless the intrinsic fluorescence of T20* and its conjugates, their interaction with membranes was also evaluated by alterations in the dipole potential.

One of the fluorescent membrane probes described as sensitive to alterations in the dipole potential is di-8-ANEPPS (*Gross et al.*, 1994).

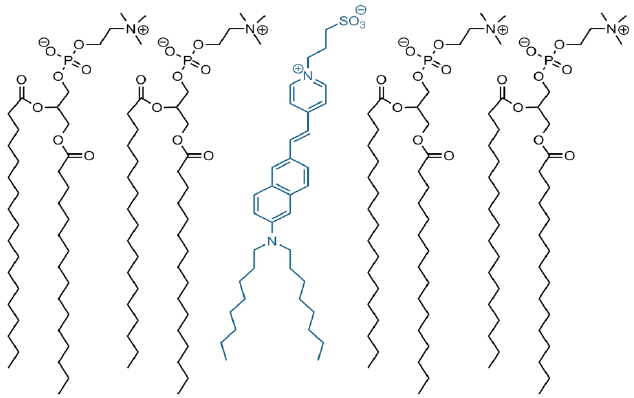

Figure 2.3 - Structure of di-8-ANEPPS (blue) between phospholipids (black).
Adapted from (*Matos et al.*, 2008).

This probe consists in two aliphatic chains, facilitating its incorporation in the outer leaflet of the membrane, attached to a chromophore region (conjugated structure) that stays nearby the lipid head-group region and senses the electric fields derived from the dipoles, acting as a reporter. This probe is believed to be electrochromic, *i.e.*, a shift in the absorption and emission spectra occur under the influence of an electric field (*Wang*, 2012). A dual wavelength ratiometric measurement can be carried with the benefit of the signal being independent of probe or cell concentrations and avoiding photobleaching artifacts. Di-8-ANEPPS can only be used as a ratiometric probe of dipole potential if the measurements are based on excitation spectrum shifts (*Vitha & Clarke*, 2007). Thus, the excitation wavelengths of 455 and 525 nm ($R = I_{455}/I_{525}$) were used and the emission wavelength was set to 670 nm in order to avoid membrane fluidity artifacts (*Clarke & Kane*, 1997; *Gross et al.*, 1994). Additionally, a large excess of lipid relative to the probes' quantity has to be used to ensure that the probe itself does not modify the dipole potential significantly (*Clarke & Kane*, 1997; *Wang*, 2012). The variation of the intensities ratio, R, with the peptide concentration can be analyzed by a single binding site model (*Cladera & O'Shea*, 1998):

$$\frac{R}{R_0} = 1 + \frac{\frac{R_{min}}{R_0}[peptide]}{K_d + [peptide]} \tag{2.7}$$

with the R values normalized for the value in the absence of the peptide, R_0. R_{min} is the asymptotic minimum value of R and K_d is the dissociation constant.

For a better observation of the excitation spectra shifts, data can be transformed in differential spectra by subtracting the normalized excitation spectra of the probe without the interacting peptide and the spectra in its presence. A sinusoidal curve with one minimum and one maximum, cutting across the x axis is obtained, as exemplified in Figure 2.4.

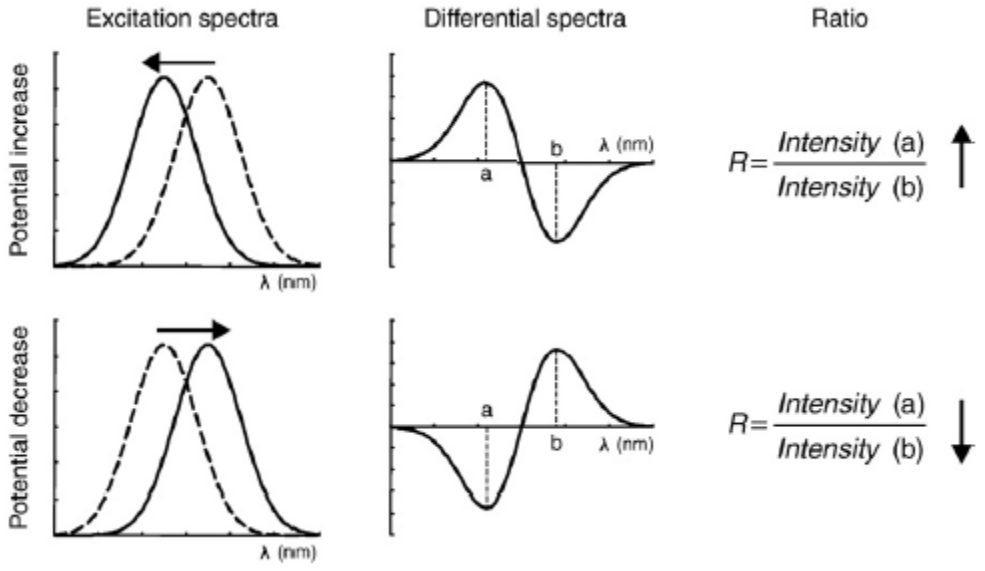

Figure 2.4 - Representation of membrane dipole potential probed by di-8-ANEPPS.
The excitation spectrum of membrane-bound di-8-ANEPPS shifts in response to changes in the dipole potential. The differential spectra help to visualize these shifts and to determine the wavelengths of maximal variation, in order to define the ratio R. Reprinted from (*Matos et al.*, 2010b)

As indicated before, the ratio of intensities,R, is calculated by the quotient of the values at two wavelengths of the differential spectra. An increase in dipole potential leads to a blue shift in the excitation spectrum, resulting in an increased ratio value. Conversely, the decreasing potential leads to a red shift and a consequent decrease of the ratio. If the dipole potential remains unchanged, as there is no interaction between the peptide and the membrane, a shift in the excitation spectra is not expected.

Membrane dipole potential on LUV

In order to assess membrane dipole potential, LUV were labeled with the probe di-8-ANEPPS. A solution containing 500 μM of freshly prepared liposomes were incubated overnight with di-8-ANEPPS 10 μM, to maximize the incorporation of the probe in the membrane. Prior to fluorescence measurements, each peptide, yielding a final concentration within a range of 0-7 μM, was incubated with di-8-ANEPPS-labeled LUV for 1 h at room temperature. Excitation spectra and the ratio of intensities at the excitation wavelengths of 455 and 525 nm ($R = I_{455}/I_{525}$) were obtained with the emission wavelength of 670 nm. Excitation and emission slits were set to 5 and 10 nm, respectively. As a control, liposomes incubated with ethanol instead of di-8-ANEPPS were also included.

Membrane dipole potential on biological samples

Erythrocytes

A 1% hematocrit suspension of erythrocytes in HEPES buffer supplemented with 0.05% Pluronic F-127, from a previously prepared 10% hematocrit sample, was used for labeling with di-8-ANEPPS 10 μM. The suspension was incubated at room temperature for 1 h, with gentle agitation and protected from light. In order to remove unbound di-8-ANEPPS, two wash cycles were performed with centrifugations at 1500 *g* for 5 min.

T20* and its derivatives, with a final concentration ranging from 0 to 6 μM, were incubated with erythrocytes at 0.02% hematocrit for 1 h and at room temperature, before fluorescence measurements. The experimental conditions of fluorescence measurements were identical to those previously described for LUV.

Peripheral blood mononuclear cells (PBMC)

PBMC were counted in a Moxi Z Mini Automated Cell Counter (ORFLO Technologies, Ketchum, ID, USA) and were prepared with a final concentration of 3000 cells/mL in 0.05% Pluronic F-127 supplemented HEPES buffer, with di-8-ANEPPS 3.3 mM. Cells' incubation with the fluorescent probe was performed during 1 h, at room temperature and protected from light. Unbound probe was washed twice with working buffer, with centrifugations at 1000 *g* for 5 min.

A concentration of 100 cells/μL was used to incubate PBMC with different concentrations of each peptide, within a range of 0-6 μM, for 1 h at room temperature. The experimental conditions of fluorescence measurements were identical to those previously described for LUV.
The variation of R with the peptide concentrations for the different types of biomembranes was analyzed by a single binding model.

Fluorescence quenching

Fluorescence quenching refers to any process that decreases the fluorescence intensity of a given substance. An array of molecular interactions such as energy transfer, ground-state complex formation, molecular rearrangements, excited-state reactions or collisional quenching can result in the decrease of a molecules' fluorescence intensity (*Lakowicz*, 2006). A quenching process, either static or dynamic, can occur if the fluorophore and the quencher are in contact with each other. In dynamic or collisional quenching, the quencher has to diffuse to the fluorophore during the lifetime of the excited state and, upon contact, the fluorophore returns to the ground state without emission of a photon. In static quenching, the fluorophore and quencher form a nonfluorescent complex. This molecular contact requirement allows the use of quenching experiments to disclose the accessibility of fluorophores to quenchers and, therefore, reveal the localization of fluorophores in proteins and membranes. If the fluorophore is located in the interior of a macromolecule, the quencher is unable to establish contact and neither collisional nor static quenching can occur (*Lakowicz*, 2006). Fluorescence's collisional quenching is described by the Stern-Volmer equation:

$$\frac{I_0}{I} = 1 + K_{sv}[Q] \qquad (2.8)$$

where I_0 and I are the fluorescence intensities in the absence and presence of quencher, respectively, K_{sv} is the Stern-Volmer constant and [Q] the concentration of quencher (*Lakowicz*, 2006). Low values of K_{sv} usually indicate that the fluorophore is inaccessible to water soluble quenchers and a higher value of this constant is an indication that the fluorophore is reachable; it could be free in solution or on the surface of a macromolecule.

Quenching by acrylamide

Acrylamide is a known quencher for tryptophan residues accessible to the aqueous environment and is useful to determine its surface accessibility. The emission spectra of 10 μM of T20* and its derivatives, incubated with POPC:Chol (2:1) liposomes with a final concentration of 3 mM, was obtained in the presence of acrylamide with a concentration ranging from 0-60 mM. An incubation time of 10 min was allowed before measurement. The same procedure was carried in the absence of LUV. An excitation wavelength of 290 nm was used in order to promote a selective excitation of tryptophan

residues. As the concentration of quencher increases, some artifacts may arise; acrylamide also absorbs at the exciting light, thus an increasing fraction of light is absorbed by the quencher and, because the overall absorption by the sample is increased, the penetration of the exciting light is less efficient, leading to a decreased fluorescence emission detection. For this reason, a correction of the fluorescence intensities by a correction factor, CF, is necessary (*Coutinho & Prieto*, 1993):

$$CF = \frac{Abs_T}{Abs_F} \times \left(\frac{1-10^{-Abs_F}}{1-10^{-Abs_T}}\right) \quad (2.9)$$

where $\mathrm{Abs_T}$ is the absorbance of the total solution and $\mathrm{Abs_F}$ is the absorbance of the fluorophore at the initial concentration. Absorption measurements were performed on a Genesys 10S UV-Vis spectrophotometer (Thermo Fisher Scientific, Madison, WI, USA) at 290 nm.
Quenching data were analyzed using the Stern-Volmer equation.

Quenching by 5NS and 16NS

Fluorescence quenching can also be a valuable tool to evaluate the depth of insertion in the membrane of a fluorophore, as an accurate determination of this parameter is an important step in protein and peptide-membrane interactions (*Ladokhin*, 2014). This can be achieved using steric acid molecules with doxyl (quencher) groups attached at different positions, such as 5-doxyl-stearic acid (5NS) and 16-doxyl-stearic acid (16NS).

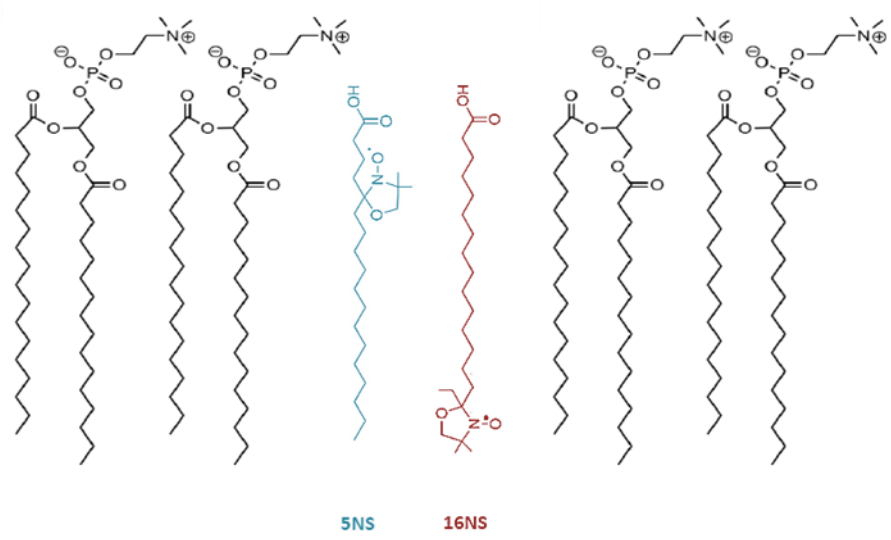

Figure 2.5 - Representation of a lipid membrane (phospholipids in black) with incorporated 5NS (blue) and 16NS (red).

As depicted in Figure 2.5, 5NS, a stearic acid with the doxyl group at carbon 5 is a better quencher for molecules in a shallow position, close to the lipid-water interface, while 16NS, a molecule with the doxyl group attached to carbon 16, is expected to quench preferentially molecules buried deeply in the membrane (*Fernandes et al.*, 2002).

An identical procedure to the quenching by acrylamide was used: a solution of each peptide (10 μM) was incubated with 3 mM POPC:Chol (2:1) LUV and successive additions of small volumes of 5NS or 16NS were made. The effective concentration of quencher at the membrane level was determined from the partition coefficient of both lipophilic molecules to biomembranes (*Santos et al.*, 1998), and range from 0 to ≈ 0.6 M. For every addition, a 10 min incubation time was allowed before measurement. The same lipid suspension was used in both cases.

Steady-state fluorescence measurements were carried out with a λ_{exc} of 280 nm and the emission spectra were recorded between 310 and 450 nm. The SIMEXDA method (*Fernandes et al.*, 2002) was applied to obtain the depth of Trp insertion in the membrane.

With the exception of ANS fluorescence, all fluorescence measurements mentioned above were conducted in a Varian Cary Eclipse fluorescence spectrophotometer (Mulgrave, Australia), with a controlled temperature of 25 ºC.

The fitting of the equations to the experimental data was done using GraphPad Prism 5.

3. Results and discussion

In previous works, it was demonstrated that the addition of a lipid moiety to a fusion inhibitor peptide increased its efficiency towards HIV-1 inhibition (*Augusto et al.*, 2014; *Hildinger et al.*, 2001; *Hollmann et al.*, 2013; *Ingallinella et al.*, 2009). Taking this into account, a previous assessment of the antiviral activity was obtained through collaboration with Prof. Matteo Porotto (Departments of Pediatrics and of Microbiology and Immunology, Weill Medical College of Cornell University, New York, USA). The conjugated peptides presented an increased antiviral activity, with an approximately 280-fold decrease of the half maximal inhibitory concentration (IC_{50}) relative to the unconjugated peptide, T20*. The antiviral activity parameters for U87 cell line, viral strain SF162 are listed in Table 3.1.

Table 3.1 – Antiviral activity of different HIV-1 fusion inhibitors (U87 cell line; viral strain SF162).

Fusion inhibitor	IC_{50} (nM)
T20*	640
T20*-Chol	2.28
T20*-PEG_4-Chol	21.8
T20*-PEG_4-Palm	2.44
T20*-Toco	6.44
T20*-PEG_4-Toco	2.48

It was reported that the addition of a cholesterol moiety to enfuvirtide decreased its antiviral affinity, suggesting that an interference between the lipid moiety and the intrinsic LBD of enfuvirtide occurs (*Ingallinella et al.*, 2009). The only difference between enfuvirtide-Chol and T20*-Chol is the peptide-lipid linker: enfuvirtide-Chol has a 4 amino acid linker while T20*-Chol has a 6 amino acid one. T20*-Chol presents the highest antiviral activity, which suggests that the 6 amino acid linker may reduce the propensity to LBD-lipid moiety interferences.

3.1. Peptide aggregation

The conjugation of peptides with lipid moieties may increase their susceptibility to aggregate in aqueous solution. For that reason, peptide aggregation was followed by ANS fluorescence.

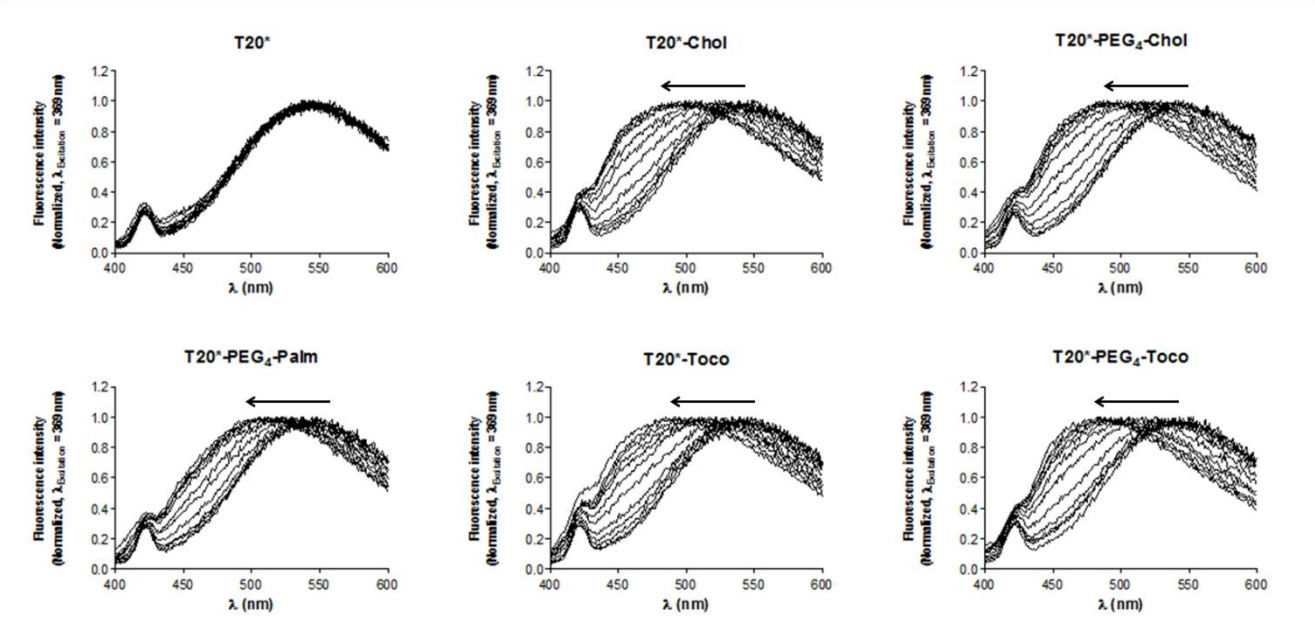

Figure 3.1 - Fluorescence spectra of ANS titrated with T20* and its derivatives.
ANS fluorescence spectra undergo a blue-shift with increasing peptide concentration (represented by the arrows).

In the presence of hydrophobic regions, ANS fluorescence emission shifts to lower wavelengths (blue shift). A blue shift is observed in the ANS' maximum fluorescence emission for all conjugated peptides (Figure 3.1), which indicates the presence of aggregates in solution. Conversely, T20* does not seem to aggregate upon increasing its concentration. In its sequence, T20* has charged residues intercalated with hydrophobic ones (Figure 2.1 – Materials and methods), which can prevent its aggregation in aqueous solution. To quantitatively differentiate the aggregation of the conjugated peptides, a fitting of the normalized fluorescence intensity data was performed (Figure 3.2). Fitting parameters are summarized in Table 3.2.

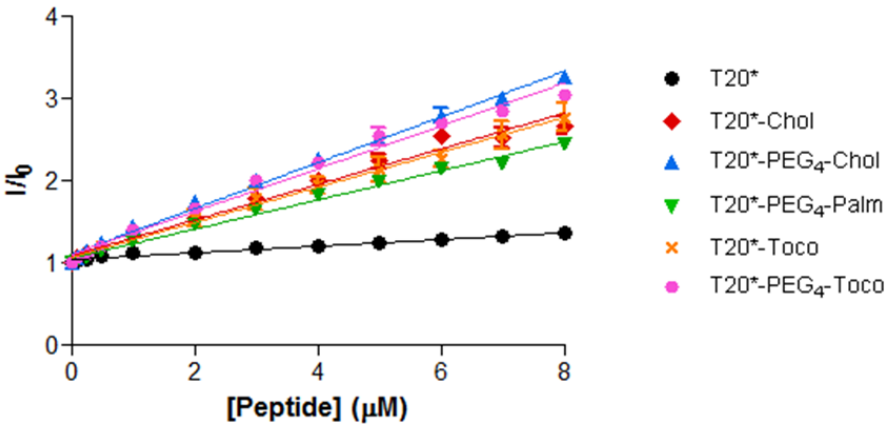

Figure 3.2 – Dependence of fluorescence intensity with peptide concentration. For each peptide, a linear regression was applied to the variation of the ratio of the fluorescence intensity in the presence of the peptide (I) and in its absence (I_0) with peptide concentration. Plotted values represent mean ± standard error of mean (SEM).

Table 3.2 – Slope, intercept and R^2 values determined from the linear fit of ANS fluorescence intensity *vs.* peptide concentration data.
The slope (m), intercept (b) and the square of the correlation coefficient (R^2) of the fit are represented for each peptide. The values represent mean ± SEM.

Peptide	m	b	R^2
T20*	0.0404 ± 0.00261	1.042 ± 0.0109	0.914
T20*-Chol	0.216 ± 0.00831	1.087 ± 0.0343	0.969
T20*-PEG$_4$-Chol	0.278 ± 0.00538	1.103 ± 0.0222	0.992
T20*-PEG$_4$-Palm	0.177 ± 0.00451	1.054 ± 0.0186	0.986
T20*-Toco	0.213 ± 0.00871	1.064 ± 0.0359	0.965
T20*-PEG$_4$-Toco	0.261 ± 0.00775	1.100 ± 0.0312	0.981

The slope of the fit confirms that T20* is the least prone to aggregation. Conversely, although all conjugated peptides tend to form aggregates, T20*-PEG$_4$-Chol and T20*-PEG$_4$-Toco have the highest propensity. Although previous studies have reported that the PEG spacer improved substantially peptide solubility in aqueous media (*Porotto et al.*, 2010), this feature was not observed for T20* conjugates.

3.2. Membrane partition

The evaluation of fusion inhibitor peptides' interaction with membranes is a key aspect of their mode of action, since the efficiency of the drug can be correlated with the membranotropic properties of the peptide (*Hollmann et al.*, 2013). Therefore the peptides' partition to biomembrane model systems was assessed by means of peptide intrinsic fluorescence. Three membrane compositions were used: POPC, to mimic the fluidity properties of biological membranes, POPC:Chol (2:1), that mimics cholesterol-rich membranes, and POPC:Chol:SM (1:1:1), in order to replicate lipid rafts.

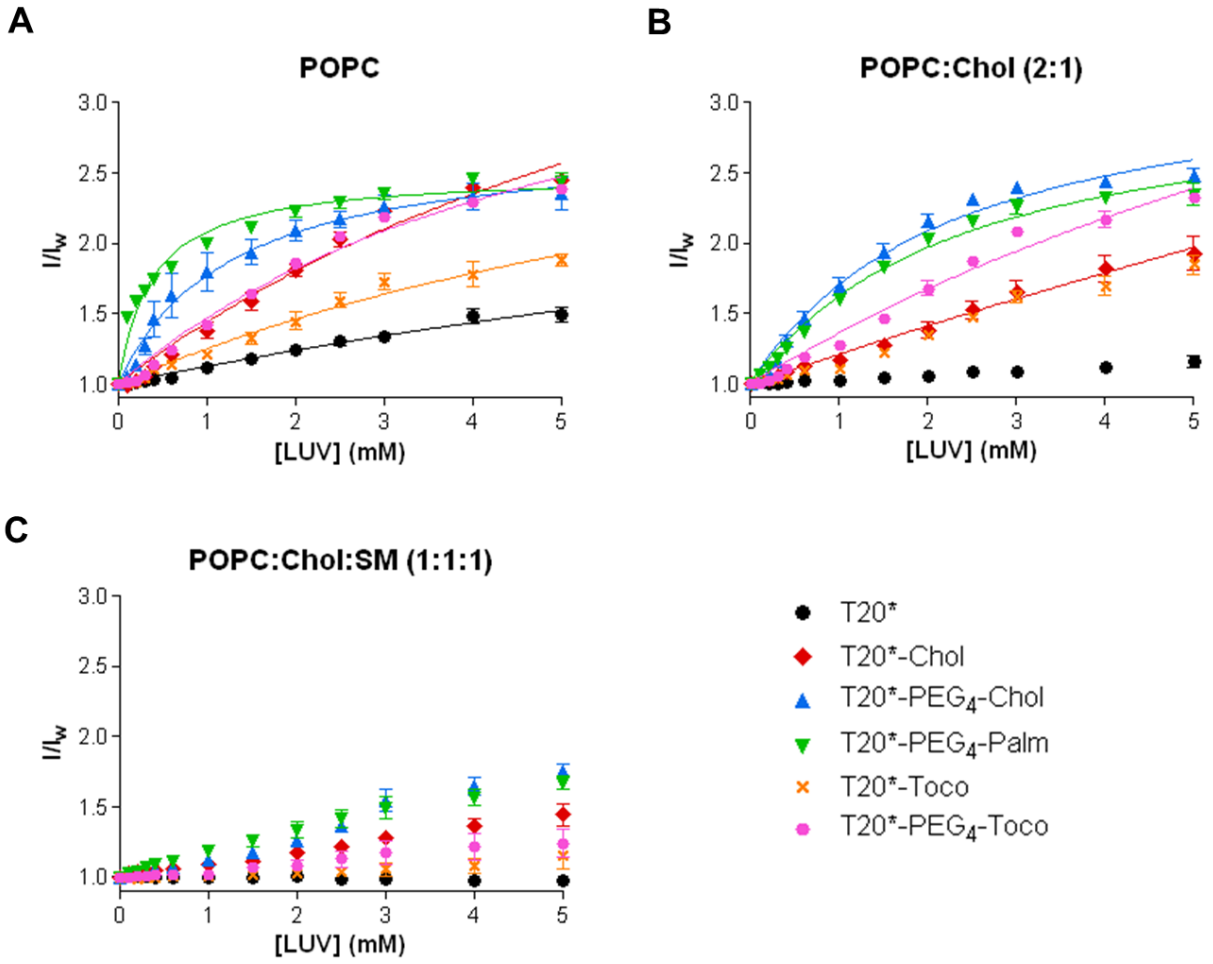

Figure 3.3 – Partition of the peptides to lipid vesicles.
Evaluation of Trp fluorescence variations of T20* derived peptides upon titration with large unilamellar vesicles (LUV), performed by successive additions of POPC (A), POPC:Chol (2:1) (B) and POPC:Chol:SM (1:1:1) (C) suspensions. Plotted values represent mean ± SEM.

The partition coefficient, K_p, for each peptide was determined from the fitting of equation 2.5 (see Materials and methods) rearranged, to the fluorescence intensities ratio (I /I_w) ratio *vs.* lipid concentration data. The K_p, and I /I_w values obtained are summarized in Table 3.3.

Table 3.3 - Partition coefficients of different fusion inhibitor peptides.
The partition coefficient (K_p) and I/I_w values were obtained from the fitting of the data obtained for T20* and its conjugates interaction with LUV of different compositions.
[a] The type of partition curve obtained impairs the use of the equation.

LUV	Peptide	K_p	I/I_w
POPC	T20*	68.85 ± 42.00	3.521 ± 1.295
	T20*-Chol	149.3 ± 33.66	5.318 ± 0.7056
	T20*-PEG_4-Chol	1037 ± 181.1	2.754 ± 0.1148
	T20*-PEG_4-Palm	3417 ± 312.8	2.500 ± 0.03414
	T20*-Toco	132.8 ± 46.48	3.736 ± 0.7134
	T20*-PEG_4-Toco	232.4 ± 35.81	4.132 ± 0.3100
POPC:Chol (2:1)	T20*	≈ 0	--
	T20*-Chol	27.38 ± 38.19	11.22 ± 13.23
	T20*-PEG_4-Chol	575.5 ± 69.56	3.318 ± 0.1315
	T20*-PEG_4-Palm	537.4 ± 57.51	3.150 ± 0.1108
	T20*-Toco	--[a]	--
	T20*-PEG_4-Toco	106.6 ± 29.60	5.799 ± 1.040
POPC:Chol:SM (1:1:1)	T20*	≈ 0	--
	T20*-Chol	--[a]	--[a]
	T20*-PEG_4-Chol		
	T20*-PEG_4-Palm		
	T20*-Toco		
	T20*-PEG_4-Toco		

In the presence of POPC vesicles, the fluorescence intensity of T20* and the conjugates increases, indicating that an interaction between the peptides and membrane takes place. In a previous work, it was reported that, for POPC membranes, enfuvirtide has a K_p of 1600 ± 100 (*Veiga et al.*, 2004a), which is much higher than the obtained for T20* (K_p = 68.85 ± 42.00). Such difference may be due to the extra 6 amino acid residues of T20*, near to Trp rich region of the peptide, which may influence its partition to membranes.

All conjugated peptides present considerably higher K_p values than T20*. PEG-containing peptides, especially T20*-PEG_4-Chol and T20*-PEG_4-Palm, have the highest values, which translates in a higher affinity of these peptides towards the membrane. Moreover, it could be expected that T20*-Chol

had a significantly higher K_p, which is not the case. This suggests that the tryptophan residues of the peptide are in a more hydrophilic environment.

Similarly to what has been reported for enfuvirtide (*Veiga et al.*, 2004a), peptides' interaction is diminished in cholesterol containing membranes. Still, T20*-PEG_4-Chol and T20*-PEG_4-Palm have the highest K_p values, suggesting that PEG may potentiate membrane partition.

Due to the type of partition curves obtained, it was not possible to determine the partition coefficients for POPC:Chol:SM membranes.

T20*-Toco and T20*-PEG_4-Toco interact with lower extent with POPC and POPC:Chol membranes and have the lowest antiviral activity amongst the conjugated peptides. Therefore, these peptides were not considered for further analysis.

3.3. Membrane dipole potential

In order to complement the membrane partition assays, which only follow the peptide Trp intrinsic fluorescence, peptide-membrane interaction was also evaluated by using the lipophilic probe di-8-ANEPPS, a fluorescent probe sensitive to the membrane dipole potential of the membrane (*Gross et al.*, 1994). The interaction of the peptides with LUV and human blood cells (PBMC and erythrocytes) was evaluated. Although peptide interaction with LUV can be characterized by their intrinsic fluorescence, this is impracticable with cells. As di-8-ANEPPS is an indirect reporter of the membrane dipole potential, any changes caused by the insertion or adsorption of the peptides can be translated in shifts in the probe's excitation spectra. In order to facilitate the visualization of the spectral shifts, differential spectra were used. The differential spectra and binding profiles of T20* and its conjugated peptides to liposomes are presented in Figure 3.4.

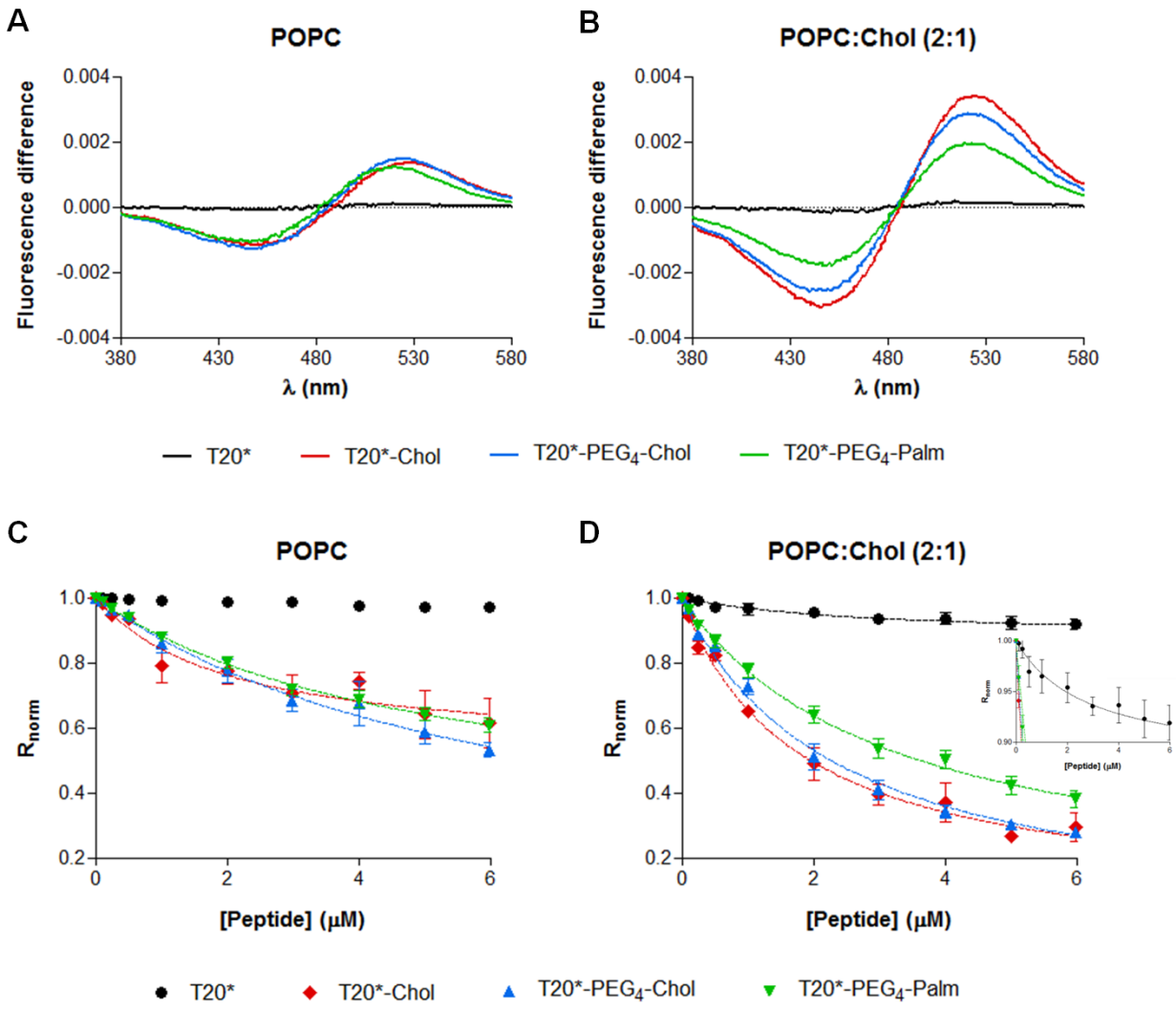

Figure 3.4 - Fusion inhibitor interactions with di-8-ANEPPS labeled LUV.
Differential spectra of POPC (A) and POPC:Chol (B) membrane-bound di-8-ANEPPS in the presence of T20*, T20*-Chol , T20*-PEG$_4$-Chol and T20*-PEG$_4$-Palm (5 μM). The binding profiles of T20* and conjugates to POPC (C) and POPC:Chol (D) are also represented, obtained by plotting the di-8-ANEPPS excitation ratio (R_{norm}) as a function of peptide concentration. (*Inset*) Binding profile of T20* to POPC:Chol (D) with a lower range of the *y* axis.

A decrease in the dipole potential is characterized by the minimum of the differential spectra to be at lower wavelengths than its maximum. This change depends on the peptide and its concentration. As it can be seen in Figure 3.4 (A, B), all T20* conjugates have a higher influence in the membrane dipole potential than T20*, in good agreement with the partition data.

In order to quantify the interaction between the peptides and the different lipid model systems, the ratio R was plotted as function of the peptide concentration (Figure 3.4 - C, D). Affinity constants can be determined by the fitting of equation 2.7 (Materials and methods) to the dipole variation curves. The obtained values are summarized in Table 3.4.

Table 3.4 - Quantification of peptide binding to LUV.
Comparison of the dissociation constant values, K_d, obtained from the binding profiles of T20* and conjugates with POPC and POPC:Chol, with the correspondent square of the correlation coefficient (R^2) of the fitted curve. Values are presented as mean ± SEM.
[a] The type of curve obtained impairs the use of the equation.

Peptide	POPC		POPC:Chol	
	K_d(μM)	R^2	K_d(μM)	R^2
T20*	--[a]	--	2.79 ± 1.53	0.704
T20*-Chol	2.06 ± 0.93	0.782	1.76 ± 0.23	0.970
T20*-PEG$_4$-Chol	6.45 ± 2.07	0.946	2.33 ± 0.23	0.985
T20*-PEG$_4$-Palm	5.12 ± 0.98	0.975	3.18 ± 0.40	0.980

The conjugated peptides present lower K_d values than the unconjugated one for POPC vesicles, which suggest that the affinity towards membranes increase with the addition of a lipid moiety, in agreement with the partition data. Regarding to POPC:Chol vesicles, although T20* presents a higher K_d value than T20*-PEG$_4$-Palm, and in spite of achieving a curve fit for the first (Figure 3.4, D - *Inset*), the correlation coefficient is fairly low (R^2 = 0.704) and for that reason the estimated K_d value might not be reliable.

Overall, the K_d value of all conjugated peptides decrease for POPC:Chol membranes in relation to POPC, suggesting a preference for cholesterol-rich membranes. Although these results are not in agreement with the partition data, it should be pointed that in the partition assays only the local changes on the Trp environment are monitored, and in this case this implies only the C-terminal region of the peptidic portion of inhibitors, whereas the dipole potential changes using di-8-ANEPPS labeled LUV are able to assess the interaction of the whole fusion inhibitor with the membrane. Thus, beside that from partition data it seems that in cholesterol-rich membranes the Trp residues are less involved in the interaction, that should not be treated as fewer interactions of the inhibitors with the membranes. An additional advantage of the dipole potential assays is that this methodology allows the evaluation of the direct interaction of the inhibitors with blood cells. In order to have a biological perspective of what may happen in the bloodstream, the interaction of the peptides with human PBMC and erythrocytes was studied (Figure 3.5).

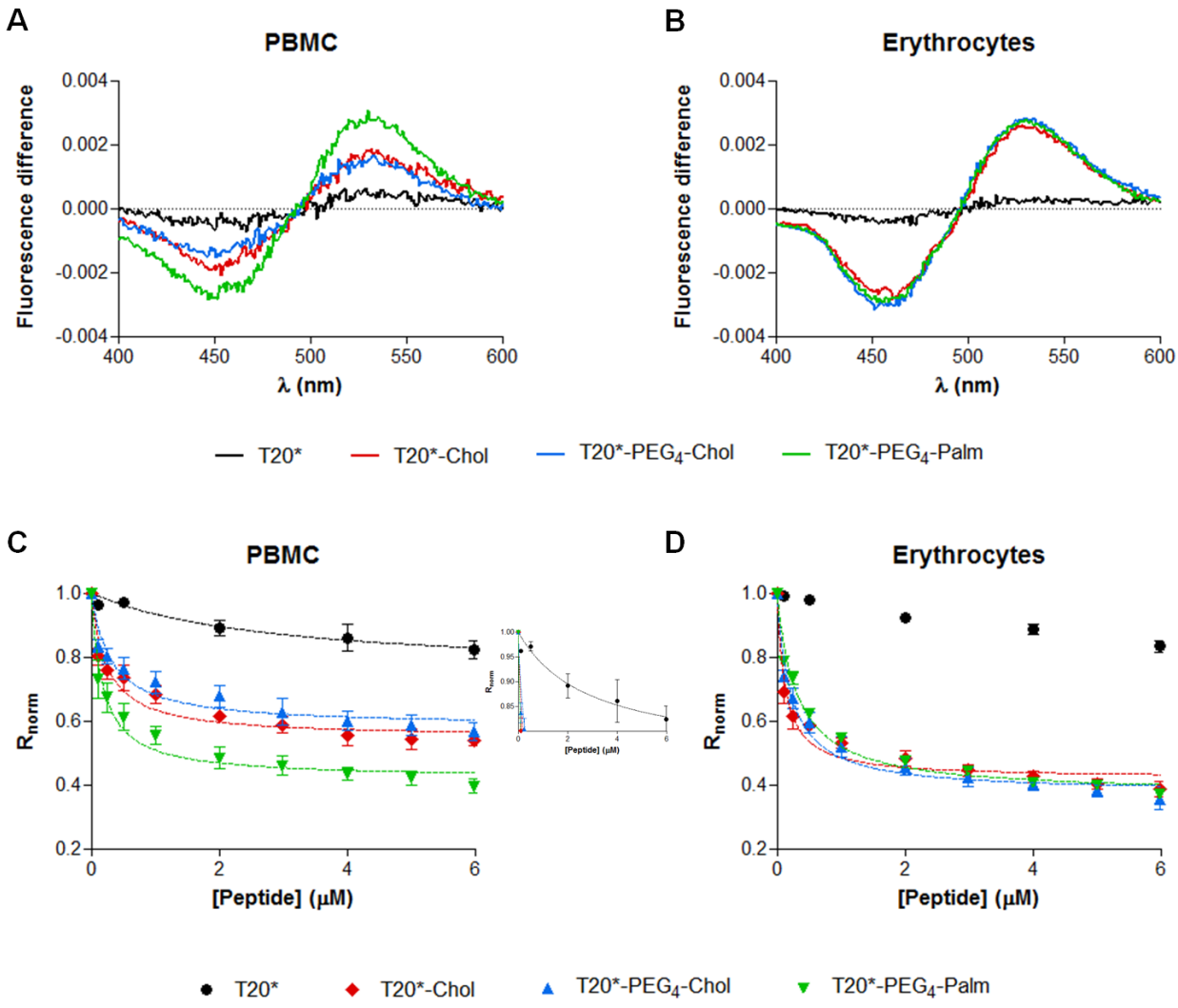

Figure 3.5 - Fusion inhibitor interactions with di-8-ANEPPS labeled cells.
Differential spectra of PBMC (A) and erythrocytes (B) membrane-bound di-8-ANEPPS in the presence of T20*, T20*-Chol, T20*-PEG$_4$-Chol and T20*-PEG$_4$-Palm (4 μM). The binding profiles of T20* and conjugates to PBMC (C) and erythrocytes (D) are also represented and were obtained by the plotting the di-8-ANEPPS excitation ratio (R_{norm}) as a function of peptide concentration. (*Inset*) Binding profile of T20* to PBMC (C) with a lower range on the *y* axis.

Similarly to the data obtained for liposome membranes, all T20* conjugates seem to cause a more pronounced decrease in the membrane potential dipole than T20*. Affinity constants can be determined for the interaction of peptides with di-8-ANEPPS labeled blood cells, and the obtained results are summarized in Table 3.5.

Table 3.5 - Quantification of peptide binding to blood cells.
Comparison of the dissociation constant values, K_d, obtained by the binding profiles of T20* and conjugates to PBMC and erythrocytes, with the correspondent square of the correlation coefficient (R^2) of the fitted curve. The values are presented as mean ± SEM.
[a] The type of curve obtained impairs the use of the equation.

Peptide	PBMC		Erythrocytes	
	K_d(μM)	R^2	K_d(μM)	R^2
T20*	2.86 ± 2.13	0.750	--[a]	--
T20*-Chol	0.239 ± 0.048	0.884	0.125 ± 0.020	0.931
T20*-PEG$_4$-Chol	0.309 ± 0.071	0.853	0.215 ± 0.030	0.943
T20*-PEG$_4$-Palm	0.181 ± 0.034	0.900	0.313 ± 0.027	0.978

Concerning the interaction of the peptides with human blood cells, all conjugated peptides exhibit higher affinity than T20*. T20*-PEG4-Palm presents the highest affinity towards PBMC, while T20*-Chol has the highest affinity to interact with erythrocytes. Overall, the conjugated peptides present a higher affinity for erythrocytes when compared to PBMC. This reinforces that the peptides may interact preferentially with cholesterol containing membranes, since erythrocytes have cholesterol-rich membranes (*Leidl et al.*, 2008).

As these peptide drugs are expected to be injected, since oral administration should not be viable, peptide binding to blood cells has high relevance.

One of HIV-1 main targets for replication and distribution all over the body are erythrocytes: it is known that the virus can associate with erythrocytes *in vivo* (*Hess et al.*, 2002) and can bind to erythrocyte membrane *in vitro* (*Beck et al.*, 2009). Moreover, trans-infection of other immune system cells present in the blood can be mediated by the erythrocytes-bound viruses (*Banki et al.*, 2006; *He et al.*, 2008a). For this reason, these cells with a pre-bound fusion inhibitor peptide could potentially restrict virus spreading through the body, and upon interaction, the virus itself could remain with the fusion peptide in its own membrane, since HIV virus and erythrocytes appear to have a similar membrane composition (*Aloia et al.*, 1988). Moreover, PBMC, which include HIV-1 preferential target cells, contribute significantly to the virus replication as it has been reported that virus bound to the surface of cells remains infectious for T cells (*Olinger et al.*, 2000).

When injected, the fusion inhibitor peptides can be dissolved in the plasma, bound to plasma proteins, and also bound to cell membranes (*Matos et al.*, 2010a). Therefore, concentrating antiretroviral peptides in cell membranes would enhance their availability towards the targets of the virus, increasing their efficiency and diminishing the amount of peptides bound to plasma proteins, which enhances drug clearance.

The availability of the fusion inhibitor peptides can also be enhanced by the addition of a PEG molecule; however, and contrary to partition data, PEG-containing peptides present a lower affinity (higher K_d) than T20*-Chol towards erythrocytes, which might suggest that the PEG spacer does not influence membrane interaction.

3.4. Localization in the lipid bilayer

In order to evaluate the location of the peptides in the membrane, we took the advantage of the quenching phenomena by using quenchers with different locations in the membrane. First, the accessibility of the tryptophan residues to the aqueous environment was evaluated by the fluorescence quenching of the peptides' intrinsic fluorescence by acrylamide. As the conjugated peptides appear to have an higher affinity towards cholesterol-rich membranes, only POPC:Chol (2:1) membranes were considered.

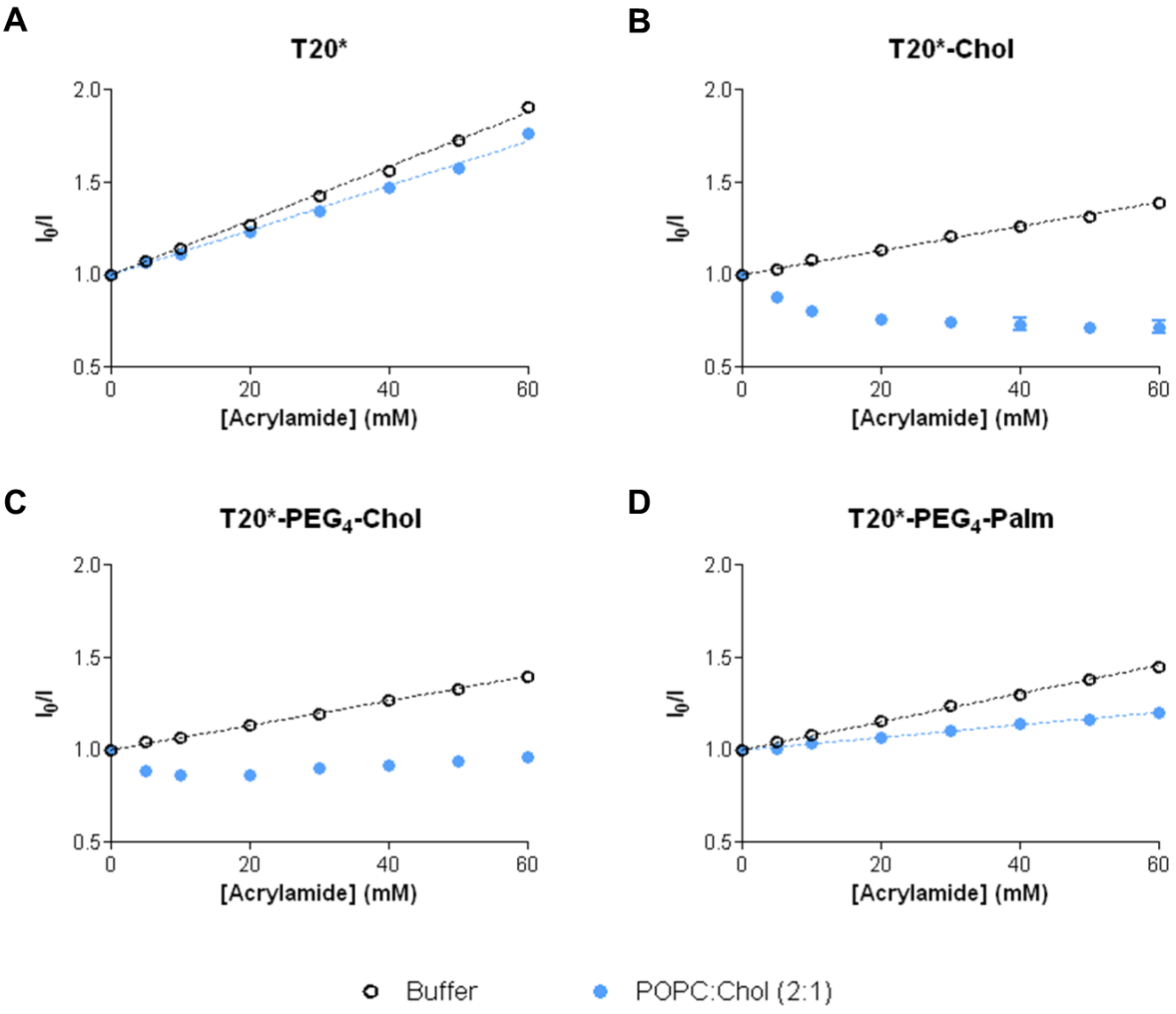

Figure 3.6 - Accessibility of the peptide to the aqueous environment.
Stern-Volmer plots of T20* and its conjugates intrinsic fluorescence quenching by the increasing concentration of acrylamide, in the absence (Buffer) and presence of LUV (POPC:Chol). Plotted values represent mean ± SEM.

The Stern-Volmer constants were obtained by the fitting of equation 2.8 (Materials and methods) to the fluorescence data.

Table 3.6 - Quantification of peptide binding.
Comparison of the values of the Stern-Volmer constant, K_{sv}, values obtained for the quenching of T20* and conjugates intrinsic fluorescence by acrylamide in the absence (buffer) and presence (POPC:Chol) of lipid. The values are presented as mean ± SEM.

Peptide	K_{sv} (M^{-1})	
	Buffer	**POPC:Chol**
T20*	14.63 ± 0.15	12.05 ± 0.16
T20*-Chol	6.56 ± 0.13	--
T20*-PEG$_4$-Chol	6.66 ± 0.18	--
T20*-PEG$_4$-Palm	7.65 ± 0.08	3.40 ± 0.14

Linear Stern-Volmer plots were obtained in the absence of lipid. By the K_{sv} values represented in Table 3.6, it is noticeable that the quenching of the conjugated peptides is less efficient than for T20*, which may indicate that the tryptophan residues are less exposed to the aqueous environment. Since conjugated peptides have lipid moieties in their structure and, as previously shown, all conjugated peptides exhibits a high tendency to aggregate, the formation of hydrophobic pockets may be the cause of such differences. In the presence of LUV, all fusion inhibitors demonstrate a reduced quenching phenomenon in comparison with the values in buffer. For the conjugated peptides containing cholesterol, T20*-Chol and T20*-PEG$_4$-Chol, a non-linear Stern-Volmer plot was obtained in the presence of LUV. The shape of the curve indicates that the fluorescence intensity exhibit a slightly increase. This may be due to conformational alterations causing tryptophan residues to be less exposed, and therefore, acrylamide is unable to quench these residues. Both T20* and T20*-PEG$_4$-Palm present K_{sv} values lower than the assay in the absence of lipid, which is indicative that these peptides interact with the membrane, although T20* in a lower extent.

The in-depth location of the tryptophan residues insertion in lipid membranes was evaluated by using lipophilic quenchers: 5NS and 16NS. The quencher group (doxyl) of these molecules, when inserted in the membrane, has distinct locations: the quencher group of 5NS locates at a shallow position, whereas 16NS quencher group locates near the hydrophobic core, deeply inside the membrane.

The Stern-Volmer plots of the fluorescence quenching by the lipophilic probes of T20* and its conjugates are presented in Figure 3.7.

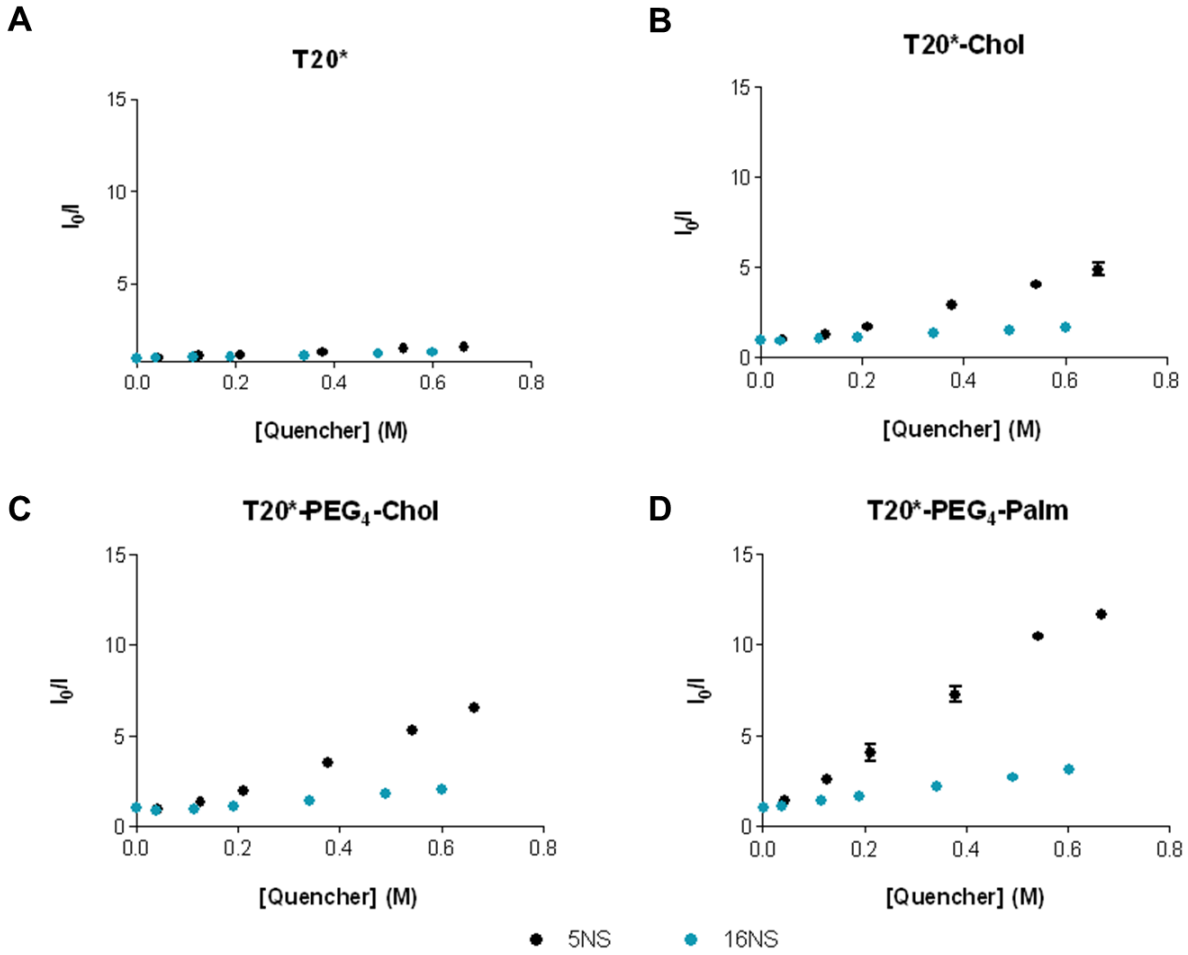

Figure 3.7 - Fluorescence quenching by lipophilic probes.
Stern-Volmer plots of the fluorescence quenching of T20* and its conjugates by the lipophilic quenchers 5NS and 16NS in POPC:Chol LUV. Plotted values represent mean ± SEM.

Overall, 5NS is a better quencher for all the T20* derived peptides, which suggests that the tryptophan residues are located in a shallow position of the membrane.

By the application of the SIMEXDA method (*Fernandes et al.*, 2002), the in-depth distribution of the fluorophores was obtained (Figure 3.8).

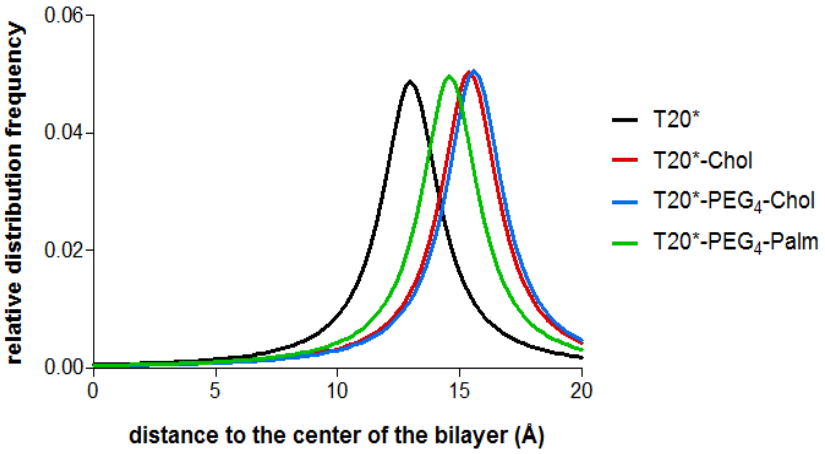

Figure 3.8 - Localization of T20* and its conjugates inside the membrane. Depth of insertion of the peptides in cholesterol-rich membranes, POPC:Chol (2:1), determined by the SIMEXDA method. The distributions' half-width at half-height were 2 Å for all peptides. The average location away from the center of the bilayer was 13 Å for T20* and 14.6 Å for T20*-PEG_4-Palm. T20*-Chol and T20*-PEG_4-Chol have a similar location of 15.4 Å and 15.6 Å, respectively.

A relatively shallow position is observed for T20* and conjugates. In average, T20* locates 13.0 Å away from the center of the bilayer, while T20*-PEG_4-Palm locates at 14.6 Å. The conjugates with cholesterol, T20*-Chol and T20*-PEG_4-Chol, locate at 15.4 Å and 15.6 Å, respectively. These results seem to disagree with the acrylamide quenching data for T20*, which suggest that the Trp residues are more exposed to the aqueous environment and, therefore, the location of the peptide is more superficial. However, the lipophilic probes 5NS and 16NS only act on peptides that are inserted in the membrane regardless of their concentration. Additionally, partition assays demonstrated that T20* interacts with the membrane in a low extent. Therefore, the 5NS and 16NS quenching data indicates that the small fraction of T20* that interacts with the membrane is inserted deeply in it. Interestingly, beside lipid conjugation boost the membrane interaction, the conjugated peptides exhibit a more shallow position in the membrane, especially in the case of cholesterol as a lipid moiety. Furthermore, PEG addition seems to have a negligible effect on the peptide location, contrary to previous results with C34-Chol (*Augusto et al.*, 2014). However, it should be pointed that in the case of the C34 conjugated peptide, the Trp region is located in the opposite region relative to the lipid moiety.

An interesting result is that T20*-Chol presented a lower membrane affinity than T20*-PEG_4-Palm, but higher than T20*-PEG_4-Chol. However, the cholesterol containing peptides are located in the same position and are more interfacial than T20*-PEG_4-Palm, nevertheless T20*-Chol exhibit the best antiviral activity (Table 3.1).

All this data confirms what was previously suggested (*Augusto et al.*, 2014), that maximizing antiviral activity requires finding the proper balance of the membrane affinity and exposure of the peptide moiety, through variations in the lipid-binding domain.

4. Conclusion

The fusion process is a key step in HIV infection, which can be targeted by fusion inhibitor peptides. Currently, enfuvirtide is the only fusion inhibitor approved for HIV-1 treatment. However, the rapid development of viral strains resistant to this inhibitor triggered the development of new peptide antiviral drugs. Fusion inhibitor peptides bind to the NHR region of gp41 in the pre-bundle configuration, *i.e.,* when the extended configuration of gp41 is bridging the viral and host membranes, before their fusion. Therefore, these peptides have a narrow time and space window of opportunity to bind to their target, which makes the aqueous diffusion of the peptide to their target less efficient. As previously reported (*Franquelim et al.*, 2008; *Hollmann et al.*, 2013; *Veiga et al.*, 2004a, 2004b), lipophilicity is an important factor for antiviral activity, since it conditions the local concentration of the fusion inhibitors at the membrane level. High antiviral activity and membranotropic behavior are related to each other, showing that the plasma membrane has an important role during the inhibition process mediated by the fusion inhibitor peptides. One of the strategies to improve the fusion inhibitors' binding to the membrane is the addition of lipid moieties to fusion peptides. This can improve the antiviral activity of fusion inhibitors, since the peptide is already present in the membrane when the virus interacts with the host cells. In previous works, it was reported that the addition of a cholesterol moiety to a fusion inhibitor, such as C34, improved its membrane interaction (especially with those containing cholesterol), and therefore its antiviral potency.

In this work, the interaction of enfuvirtide-derived peptides, by the conjugation with lipid anchors and using PEG and 6 additional amino acid residues in between, towards biomembrane model systems and human blood cells as a biological model for what may happen in the bloodstream, was assessed.

The addition of lipid moieties to T20* increased its antiviral potency, and partition data showed that there were also an increased binding of all conjugated peptides to membranes. However, a detailed analysis of the partition data towards membranes with different compositions reveals differences between the conjugated peptides. Besides, and in all the cases, conjugated peptides exhibit higher partition coefficients than T20*. K_p values decreased when cholesterol membranes were tested, meaning that the tryptophan region is less involved in the membrane interaction in those compounds.

In order to complement partition data, fusion inhibitors interaction with membranes were also evaluated following the dipole potential changes using di-8-ANEPPS labeled LUV. Unlike the behavior observed with partition assays, T20* and its conjugates decreased in a greater extent the membrane dipole potential of POPC:Chol membranes, when compared with POPC. As lipid rafts are essential for the HIV entry process, the high affinity of T20* conjugates towards cholesterol-rich domains would concentrate the drug where HIV fusion is likely to occur. Erythrocytes and PBMC are the main targets of the virus for distribution and replication all over the body, respectively. In this context, the interactions of inhibitors with these two types of cells were also evaluated by measuring dipole potential changes. Similarly to LUV results, T20* conjugates presented a higher affinity than unconjugated T20* for both human blood cells.

Overall, fluorescence quenching assays revealed that T20* conjugated peptides interact with POPC:Chol membranes and their tryptophan residues locate in a more shallow position within the membrane than the unconjugated peptide. These fluorophores are more exposed to the aqueous

environment, and therefore the peptidic portion of the inhibitors is more available to interact with the virus.

Regarding the different lipid moieties tested, besides all of them being able to boost membrane affinity, cholesterol seems to be the one that provides the best balance between membrane anchoring and exposure. Additionally, although it has been reported that PEG addition to fusion inhibitors increases its antiviral activity and affinity towards membranes, the results obtained here were inconclusive at that level.

Although a further characterization of the peptides' membranotropic properties is necessary, the results obtained allow to conclude that a proper balance between membrane affinity and exposure of the peptide is required in order to enhance antiviral activity. The addition of lipid moieties to an established fusion inhibitor, such as enfuvirtide, can be a promising strategy against HIV.

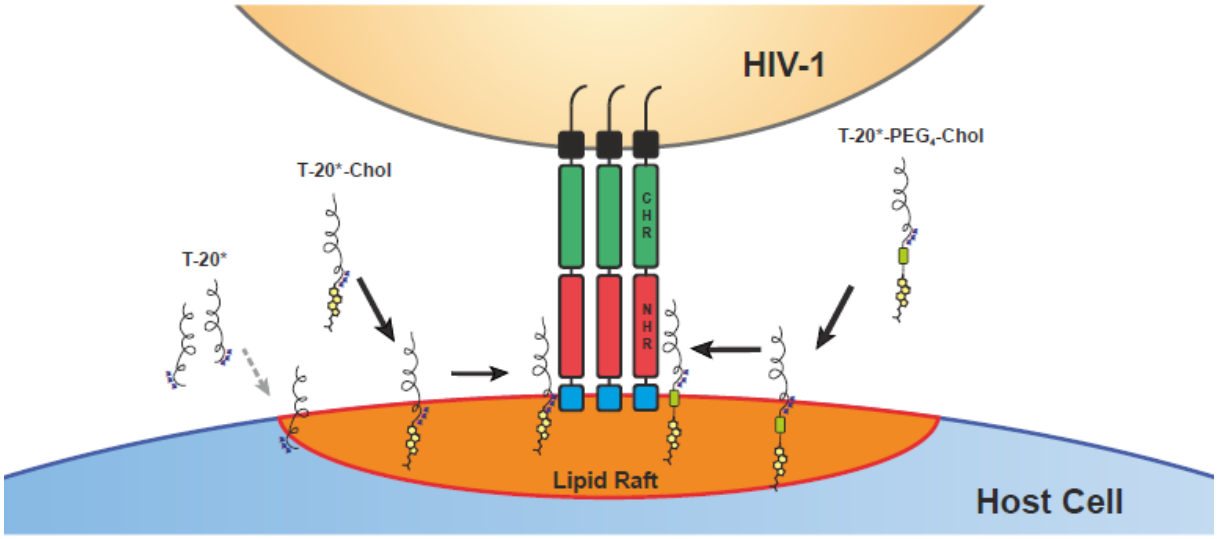

Figure 3.9 - Putative role of action of HIV-1 fusion inhibitors T20*-Chol and T20*-PEG$_4$-Chol.
T20* lipid conjugated peptides anchor to the membrane via their cholesterol moiety. In the context of HIV-1 gp41 engagement with the target cell, a confined space exists between the two membranes. The drug concentrated in the lipid raft environment may reach its target (gp41 during its extended conformation) more efficiently than simple diffusion in aqueous solution. Moreover, the anchoring promoted by the cholesterol at the C-terminal and the higher exposition of the PBD to aqueous media, brings the peptide into contact in the correct orientation to compete with the NHR binding site. This way, gp41 mediated fusion may be inhibited, blocking viral content entry into the cell.

References

Adamson, C. S., & Freed, E. O. (2010). Novel approaches to inhibiting HIV-1 replication. *Antiviral Research*, *85*(1), 119–41.

Aloia, R. C., Jensen, F. C., Curtain, C. C., Mobley, P. W., & Gordon, L. M. (1988). Lipid composition and fluidity of the human immunodeficiency virus. *Proceedings of the National Academy of Sciences*, *85*(3), 900–904.

Augusto, M. T., Hollmann, A., Castanho, M. A. R. B., Porotto, M., Pessi, A., & Santos, N. C. (2014). Improvement of HIV fusion inhibitor C34 efficacy by membrane anchoring and enhanced exposure. *The Journal of Antimicrobial Chemotherapy*, *69*(5), 1286–97.

Banki, Z., Wilflingseder, D., Ammann, C. G., Pruenster, M., Mullauer, B., Hollander, K., Meyer, M., Sprinzl, G. M., van Lunzen, J., Stellbrink, H.-J., Dierich, M. P., & Stoiber, H. (2006). Factor I-Mediated Processing of Complement Fragments on HIV Immune Complexes Targets HIV to CR2-Expressing B Cells and Facilitates B Cell-Mediated Transmission of Opsonized HIV to T Cells. *The Journal of Immunology*, *177*(5), 3469–3476.

Barré-Sinoussi, F., Chermann, J., Rey, F., Nugeyre, M., Chamaret, S., Gruest, J., Dauguet, C., Axler-Blin, C., Vezinet-Brun, F., Rouzioux, C., Rozenbaum, W., & Montagnier, L. (1983). Isolation of a T-lymphotropic retrovirus from a patient at risk for acquired immune deficiency syndrome (AIDS). *Science*, *220*(4599), 868–871.

Beck, Z., Brown, B. K., Wieczorek, L., Peachman, K. K., Matyas, G. R., Polonis, V. R., Rao, M., & Alving, C. R. (2009). Human erythrocytes selectively bind and enrich infectious HIV-1 virions. *PloS One*, *4*(12), e8297.

Berkhout, B., Eggink, D., & Sanders, R. W. (2012). Is there a future for antiviral fusion inhibitors? *Current Opinion in Virology*, *2*(1), 50–9.

Blumenthal, R., Durell, S., & Viard, M. (2012). HIV entry and envelope glycoprotein-mediated fusion. *The Journal of Biological Chemistry*, *287*(49), 40841–9.

Brügger, B., Glass, B., Haberkant, P., Leibrecht, I., Wieland, F. T., & Kräusslich, H.-G. (2006). The HIV lipidome: a raft with an unusual composition. *Proceedings of the National Academy of Sciences of the United States of America*, *103*(8), 2641–6.

Burton, D. R., Desrosiers, R. C., Doms, R. W., Koff, W. C., Kwong, P. D., Moore, J. P., Nabel, G. J., Sodroski, J., Wilson, I. a, & Wyatt, R. T. (2004). HIV vaccine design and the neutralizing antibody problem. *Nature Immunology*, *5*(3), 233–6.

Chan, D. C., Chutkowski, C. T., & Kim, P. S. (1998). Evidence that a prominent cavity in the coiled coil of HIV type 1 gp41 is an attractive drug target. *Proceedings of the National Academy of Sciences*, *95*(26), 15613–15617.

Chan, D. C., Fass, D., Berger, J. M., & Kim, P. S. (1997). Core Structure of gp41 from the HIV Envelope Glycoprotein. *Cell*, *89*(2), 263–273.

Cladera, J., & O'Shea, P. (1998). Intramembrane molecular dipoles affect the membrane insertion and folding of a model amphiphilic peptide. *Biophysical Journal*, *74*(5), 2434–42.

Clarke, R. J., & Kane, D. J. (1997). Optical detection of membrane dipole potential: avoidance of fluidity and dye-induced effects. *Biochimica et Biophysica Acta*, *1323*(2), 223–39.

Coffin, J., Haase, A., Levy, J. A., Montagnier, L., Oroszlan, S., Teich, N., Temin, H., Toyoshima, K., Varmus, H., & Vogt, P. (1986). Human immunodeficiency viruses. *Science (New York, N.Y.)*, *232*(4751), 697.

Coutinho, A., & Prieto, M. (1993). Ribonuclease T1 and alcohol dehydrogenase fluorescence quenching by acrylamide: A laboratory experiment for undergraduate students. *Journal of Chemical Education*, *70*(5), 425.

Davis, K. C. (1983). Acquired Immunodeficiency Syndrome in a Patient with Hemophilia. *Annals of Internal Medicine*, *98*(3), 284.

De Clercq, E. (2009). Anti-HIV drugs: 25 compounds approved within 25 years after the discovery of HIV. *International Journal of Antimicrobial Agents*, *33*(4), 307–20.

De Clercq, E. (2013). Antivirals: past, present and future. *Biochemical Pharmacology*, *85*(6), 727–44.

Doms, R. W., & Trono, D. (2000). The plasma membrane as a combat zone in the HIV battlefield. *Genes & Development*, *14*(21), 2677–2688.

Engelman, A., & Cherepanov, P. (2012). The structural biology of HIV-1: mechanistic and therapeutic insights. *Nature Reviews. Microbiology*, *10*(4), 279–90.

Eron, J. J., Gulick, R. M., Bartlett, J. A., Merigan, T., Arduino, R., Kilby, J. M., Yangco, B., Diers, A., Drobnes, C., DeMasi, R., Greenberg, M., Melby, T., Raskino, C., Rusnak, P., Zhang, Y., Spence, R., & Miralles, G. D. (2004). Short-term safety and antiretroviral activity of T-1249, a second-generation fusion inhibitor of HIV. *The Journal of Infectious Diseases*, *189*(6), 1075–83.

Fernandes, M. X., García de la Torre, J., & Castanho, M. A. R. B. (2002). Joint determination by Brownian dynamics and fluorescence quenching of the in-depth location profile of biomolecules in membranes. *Analytical Biochemistry*, *307*(1), 1–12.

Franquelim, H. G., Loura, L. M. S., Santos, N. C., & Castanho, M. A. R. B. (2008). Sifuvirtide screens rigid membrane surfaces. establishment of a correlation between efficacy and membrane domain selectivity among HIV fusion inhibitor peptides. *Journal of the American Chemical Society*, *130*(19), 6215–23.

Franquelim, H. G., Matos, P. M., & Veiga, A. S. (2011). HIV vs. HIV: Turning HIV-Derived Peptides into Drugs. In M. Castanho & N. C. Santos (Eds.), *Peptide Drug Discovery and Development*. Weinheim, Germany: Wiley-VCH Verlag GmbH & Co. KGaA.

Gottlieb, M. S., Schroff, R., Schanker, H. M., Weisman, J. D., Fan, P. T., Wolf, R. A., & Saxon, A. (1981). Pneumocystis carinii Pneumonia and Mucosal Candidiasis in Previously Healthy Homosexual Men. *New England Journal of Medicine*, *305*(24), 1425–1431.

Greenberg, M. L., & Cammack, N. (2004). Resistance to enfuvirtide, the first HIV fusion inhibitor. *The Journal of Antimicrobial Chemotherapy*, *54*(2), 333–40.

Gross, E., Bedlack, R. S., & Loew, L. M. (1994). Dual-wavelength ratiometric fluorescence measurement of the membrane dipole potential. *Biophysical Journal*, *67*(1), 208–16.

Hallenberger, S., Bosch, V., Angliker, H., Shaw, E., Klenk, H. D., & Garten, W. (1992). Inhibition of furin-mediated cleavage activation of HIV-1 glycoprotein gp160. *Nature*, *360*(6402), 358–61.

Haqqani, A. a, & Tilton, J. C. (2013). Entry inhibitors and their use in the treatment of HIV-1 infection. *Antiviral Research*, *98*(2), 158–70.

He, W., Neil, S., Kulkarni, H., Wright, E., Agan, B. K., Marconi, V. C., Dolan, M. J., Weiss, R. A., & Ahuja, S. K. (2008a). Duffy antigen receptor for chemokines mediates trans-infection of HIV-1 from red blood cells to target cells and affects HIV-AIDS susceptibility. *Cell Host & Microbe*, *4*(1), 52–62.

He, Y., Xiao, Y., Song, H., Liang, Q., Ju, D., Chen, X., Lu, H., Jing, W., Jiang, S., & Zhang, L. (2008b). Design and evaluation of sifuvirtide, a novel HIV-1 fusion inhibitor. *The Journal of Biological Chemistry*, *283*(17), 11126–34.

Hemelaar, J. (2012). The origin and diversity of the HIV-1 pandemic. *Trends in Molecular Medicine*, *18*(3), 182–92.

Hemelaar, J. (2013). Implications of HIV diversity for the HIV-1 pandemic. *The Journal of Infection*, *66*(5), 391–400.

Henrich, T. J., & Kuritzkes, D. R. (2013). HIV-1 entry inhibitors: recent development and clinical use. *Current Opinion in Virology*, *3*(1), 51–7.

Henriques, S. T., Pattenden, L. K., Aguilar, M.-I., & Castanho, M. a R. B. (2008). PrP(106-126) does not interact with membranes under physiological conditions. *Biophysical Journal*, *95*(4), 1877–89.

Hess, C., Klimkait, T., Schlapbach, L., Del Zenero, V., Sadallah, S., Horakova, E., Balestra, G., Werder, V., Schaefer, C., Battegay, M., & Schifferli, J.-A. (2002). Association of a pool of HIV-1 with erythrocytes in vivo: a cohort study. *Lancet*, *359*(9325), 2230–4.

Hildinger, M., Dittmar, M. T., Schult-Dietrich, P., Fehse, B., Schnierle, B. S., Thaler, S., Stiegler, G., Welker, R., & von Laer, D. (2001). Membrane-anchored peptide inhibits human immunodeficiency virus entry. *Journal of Virology*, *75*(6), 3038–42.

Hollmann, A., Matos, P. M., Augusto, M. T., Castanho, M. a R. B., & Santos, N. C. (2013). Conjugation of cholesterol to HIV-1 fusion inhibitor C34 increases peptide-membrane interactions potentiating its action. *PloS One*, *8*(4), e60302.

Ingallinella, P., Bianchi, E., Ladwa, N. a, Wang, Y.-J., Hrin, R., Veneziano, M., Bonelli, F., Ketas, T. J., Moore, J. P., Miller, M. D., & Pessi, A. (2009). Addition of a cholesterol group to an HIV-1 peptide fusion inhibitor dramatically increases its antiviral potency. *Proceedings of the National Academy of Sciences of the United States of America*, *106*(14), 5801–6.

Jevsevar, S., Kunstelj, M., & Porekar, V. G. (2010). PEGylation of therapeutic proteins. *Biotechnology Journal*, *5*(1), 113–28.

Jiang, S., Lin, K., Strick, N., & Neurath, A. R. (1993). HIV-1 inhibition by a peptide. *Nature*, *365*(6442), 113.

Karlsson Hedestam, G. B., Fouchier, R. A. M., Phogat, S., Burton, D. R., Sodroski, J., & Wyatt, R. T. (2008). The challenges of eliciting neutralizing antibodies to HIV-1 and to influenza virus. *Nature Reviews. Microbiology*, *6*(2), 143–55.

Klasse, P. J. (2012). The molecular basis of HIV entry. *Cellular Microbiology*, *14*(8), 1183–92.

Ladokhin, A. S. (2014). Measuring membrane penetration with depth-dependent fluorescence quenching: distribution analysis is coming of age. *Biochimica et Biophysica Acta*, *1838*(9), 2289–95.

Ladokhin, A. S., Jayasinghe, S., & White, S. H. (2000). How to measure and analyze tryptophan fluorescence in membranes properly, and why bother? *Analytical Biochemistry*, *285*(2), 235–45.

Lakowicz, J. R. (2006). *Principles of Fluorescence Spectroscopy* (3rd ed.). Boston, MA: Springer US.

Leidl, K., Liebisch, G., Richter, D., & Schmitz, G. (2008). Mass spectrometric analysis of lipid species of human circulating blood cells. *Biochimica et Biophysica Acta*, *1781*(10), 655–64.

Lieberman-Blum, S. S., Fung, H. B., & Bandres, J. C. (2008). Maraviroc: A CCR5-receptor antagonist for the treatment of HIV-1 infection. *Clinical Therapeutics*, *30*(7), 1228–1250.

Liu, S., Jing, W., Cheung, B., Lu, H., Sun, J., Yan, X., Niu, J., Farmar, J., Wu, S., & Jiang, S. (2007). HIV gp41 C-terminal heptad repeat contains multifunctional domains. Relation to mechanisms of action of anti-HIV peptides. *The Journal of Biological Chemistry*, *282*(13), 9612–20.

Liu, S., Lu, H., Niu, J., Xu, Y., Wu, S., & Jiang, S. (2005). Different from the HIV fusion inhibitor C34, the anti-HIV drug Fuzeon (T-20) inhibits HIV-1 entry by targeting multiple sites in gp41 and gp120. *The Journal of Biological Chemistry*, *280*(12), 11259–73.

Liu, S.-Y., Aliyari, R., Chikere, K., Li, G., Marsden, M. D., Smith, J. K., Pernet, O., Guo, H., Nusbaum, R., Zack, J. a, Freiberg, A. N., Su, L., Lee, B., & Cheng, G. (2013). Interferon-inducible cholesterol-25-hydroxylase broadly inhibits viral entry by production of 25-hydroxycholesterol. *Immunity*, *38*(1), 92–105.

Locher, C. P., Witt, S. a, Kassel, R., Dowell, N. L., Fujimura, S., & Levy, J. a. (2005). Differential effects of R5 and X4 human immunodeficiency virus type 1 infection on CD4+ cell proliferation and activation. *The Journal of General Virology*, *86*(Pt 4), 1171–9.

Lorizate, M., Huarte, N., Sáez-Cirión, A., & Nieva, J. L. (2008). Interfacial pre-transmembrane domains in viral proteins promoting membrane fusion and fission. *Biochimica et Biophysica Acta*, *1778*(7-8), 1624–39.

Madsen, K., Knudsen, L. B., Agersoe, H., Nielsen, P. F., Thøgersen, H., Wilken, M., & Johansen, N. L. (2007). Structure-activity and protraction relationship of long-acting glucagon-like peptide-1 derivatives: importance of fatty acid length, polarity, and bulkiness. *Journal of Medicinal Chemistry*, *50*(24), 6126–32.

Markosyan, R. M., Cohen, F. S., & Melikyan, G. B. (2003). HIV-1 envelope proteins complete their folding into six-helix bundles immediately after fusion pore formation. *Molecular Biology of the Cell*, *14*(3), 926–38.

Martin-Carbonero, L. (2004). Discontinuation of the clinical development of fusion inhibitor T-1249. *AIDS Reviews*, *6*(1), 61.

Masur, H., Michelis, M. A., Greene, J. B., Onorato, I., Stouwe, R. A., Holzman, R. S., Wormser, G., Brettman, L., Lange, M., Murray, H. W., & Cunningham-Rundles, S. (1981). An outbreak of community-acquired Pneumocystis carinii pneumonia: initial manifestation of cellular immune dysfunction. *The New England Journal of Medicine*, *305*(24), 1431–8.

Matos, P. M., Castanho, M. a R. B., & Santos, N. C. (2010a). HIV-1 fusion inhibitor peptides enfuvirtide and T-1249 interact with erythrocyte and lymphocyte membranes. *PloS One*, *5*(3), e9830.

Matos, P. M., Franquelim, H. G., Castanho, M. a R. B., & Santos, N. C. (2010b). Quantitative assessment of peptide-lipid interactions. Ubiquitous fluorescence methodologies. *Biochimica et Biophysica Acta*, *1798*(11), 1999–2012.

Matos, P. M., Gonçalves, S., & Santos, N. C. (2008). Interaction of peptides with biomembranes assessed by potential-sensitive fluorescent probes. *Journal of Peptide Science : An Official Publication of the European Peptide Society*, *14*(4), 407–15.

Matthews, T., Salgo, M., Greenberg, M., Chung, J., DeMasi, R., & Bolognesi, D. (2004). Enfuvirtide: the first therapy to inhibit the entry of HIV-1 into host CD4 lymphocytes. *Nature Reviews. Drug Discovery*, *3*(3), 215–25.

Mayer, L. D., Hope, M. J., & Cullis, P. R. (1986). Vesicles of variable sizes produced by a rapid extrusion procedure. *Biochimica et Biophysica Acta (BBA) - Biomembranes*, *858*(1), 161–168.

Münch, J., Ständker, L., Adermann, K., Schulz, A., Schindler, M., Chinnadurai, R., Pöhlmann, S., Chaipan, C., Biet, T., Peters, T., Meyer, B., Wilhelm, D., Lu, H., Jing, W., Jiang, S., Forssmann, W.-G., & Kirchhoff, F. (2007). Discovery and optimization of a natural HIV-1 entry inhibitor targeting the gp41 fusion peptide. *Cell*, *129*(2), 263–75.

Murphy, K. M. (2011). *Janeways's immunobiology* (8th ed., p. 888). Garland Science.

Olinger, G. G., Saifuddin, M., & Spear, G. T. (2000). CD4-Negative Cells Bind Human Immunodeficiency Virus Type 1 and Efficiently Transfer Virus to T Cells. *Journal of Virology*, *74*(18), 8550–8557.

Otaka, A., Nakamura, M., Nameki, D., Kodama, E., Uchiyama, S., Nakamura, S., Nakano, H., Tamamura, H., Kobayashi, Y., Matsuoka, M., & Fujii, N. (2002). Remodeling of gp41-C34 peptide leads to highly effective inhibitors of the fusion of HIV-1 with target cells. *Angewandte Chemie (International Ed. in English)*, *41*(16), 2937–40.

Podbilewicz, B. (2014). Virus and Cell Fusion Mechanisms. *Annual Review of Cell and Developmental Biology*, (June), 1–29.

Porotto, M., Rockx, B., Yokoyama, C. C., Talekar, A., Devito, I., Palermo, L. M., Liu, J., Cortese, R., Lu, M., Feldmann, H., Pessi, A., & Moscona, A. (2010). Inhibition of Nipah virus infection in vivo: targeting an early stage of paramyxovirus fusion activation during viral entry. *PLoS Pathogens*, *6*(10), e1001168.

Reardon, P. N., Sage, H., Dennison, S. M., Martin, J. W., Donald, B. R., Alam, S. M., Haynes, B. F., & Spicer, L. D. (2014). Structure of an HIV-1-neutralizing antibody target, the lipid-bound gp41 envelope membrane proximal region trimer. *Proceedings of the National Academy of Sciences of the United States of America*, *111*(4), 1391–6.

Reeves, J. D., & Doms, R. W. (2002). Human immunodeficiency virus type 2. *The Journal of General Virology*, *83*(Pt 6), 1253–65.

Santos, N. C. (2003). Quantifying molecular partition into model systems of biomembranes: an emphasis on optical spectroscopic methods. *Biochimica et Biophysica Acta (BBA) - Biomembranes*, *1612*(2), 123–135.

Santos, N. C., Prieto, M., & Castanho, M. a. (1998). Interaction of the major epitope region of HIV protein gp41 with membrane model systems. A fluorescence spectroscopy study. *Biochemistry*, *37*(24), 8674–82.

Sougrat, R., Bartesaghi, A., Lifson, J. D., Bennett, A. E., Bess, J. W., Zabransky, D. J., & Subramaniam, S. (2007). Electron tomography of the contact between T cells and SIV/HIV-1: implications for viral entry. *PLoS Pathogens*, *3*(5), e63.

St Vincent, M. R., Colpitts, C. C., Ustinov, A. V, Muqadas, M., Joyce, M. a, Barsby, N. L., Epand, R. F., Epand, R. M., Khramyshev, S. a, Valueva, O. a, Korshun, V. a, Tyrrell, D. L. J., & Schang, L. M. (2010). Rigid amphipathic fusion inhibitors, small molecule antiviral compounds against enveloped viruses. *Proceedings of the National Academy of Sciences of the United States of America*, *107*(40), 17339–44.

Steffen, I., & Pöhlmann, S. (2010). Peptide-based inhibitors of the HIV envelope protein and other class I viral fusion proteins. *Current Pharmaceutical Design*, *16*(9), 1143–58.

Tilton, J. C., & Doms, R. W. (2010). Entry inhibitors in the treatment of HIV-1 infection. *Antiviral Research*, *85*(1), 91–100.

Tözsér, J. (2003). Stages of HIV replication and targets for therapeutic intervention. *Current Topics in Medicinal Chemistry*, *3*(13), 1447–57.

UNAIDS. (2014). The gap report. Retrieved from http://www.unaids.org/

Veiga, S., Henriques, S., Santos, N. C., & Castanho, M. (2004a). Putative role of membranes in the HIV fusion inhibitor enfuvirtide mode of action at the molecular level. *The Biochemical Journal*, *377*(Pt 1), 107–10.

Veiga, S., Santos, N. C., Loura, L. M. S., Fedorov, A., & Castanho, M. A. R. B. (2004b). HIV fusion inhibitor peptide T-1249 is able to insert or adsorb to lipidic bilayers. Putative correlation with improved efficiency. *Journal of the American Chemical Society*, *126*(45), 14758–63.

Vigant, F., Hollmann, A., Lee, J., Santos, N. C., Jung, M. E., & Lee, B. (2014). The rigid amphipathic fusion inhibitor dUY11 acts through photosensitization of viruses. *Journal of Virology*, *88*(3), 1849–53.

Vigant, F., Lee, J., Hollmann, A., Tanner, L. B., Akyol Ataman, Z., Yun, T., Shui, G., Aguilar, H. C., Zhang, D., Meriwether, D., Roman-Sosa, G., Robinson, L. R., Juelich, T. L., Buczkowski, H., Chou, S., Castanho, M. a R. B., Wolf, M. C., Smith, J. K., Banyard, A., Kielian, M., Reddy, S., Wenk, M. R., Selke, M., Santos, N. C., Freiberg, A. N., Jung, M. E., & Lee, B. (2013). A mechanistic paradigm for broad-spectrum antivirals that target virus-cell fusion. *PLoS Pathogens*, *9*(4), e1003297.

Vitha, M. F., & Clarke, R. J. (2007). Comparison of excitation and emission ratiometric fluorescence methods for quantifying the membrane dipole potential. *Biochimica et Biophysica Acta*, *1768*(1), 107–14.

Wang, L. (2012). Measurements and implications of the membrane dipole potential. *Annual Review of Biochemistry*, *81*, 615–35.

Weiss, R. A. (2000). Getting to know HIV. *Tropical Medicine & International Health : TM & IH*, *5*(7), A10–5.

Wild, C., Oas, T., McDanal, C., Bolognesi, D., & Matthews, T. (1992). A synthetic peptide inhibitor of human immunodeficiency virus replication: correlation between solution structure and viral inhibition. *Proceedings of the National Academy of Sciences*, *89*(21), 10537–10541.

Wilen, C. B., Tilton, J. C., & Doms, R. W. (2012). Molecular mechanisms of HIV Entry. In M. G. Rossmann & V. B. Rao (Eds.), (Vol. 726, pp. 223–242). Boston, MA: Springer US.

Worobey, M., Gemmel, M., Teuwen, D. E., Haselkorn, T., Kunstman, K., Bunce, M., Muyembe, J.-J., Kabongo, J.-M. M., Kalengayi, R. M., Van Marck, E., Gilbert, M. T. P., & Wolinsky, S. M. (2008). Direct evidence of extensive diversity of HIV-1 in Kinshasa by 1960. *Nature*, *455*(7213), 661–4.

Wyatt, R. (1998). The HIV-1 Envelope Glycoproteins: Fusogens, Antigens, and Immunogens. *Science*, *280*(5371), 1884–1888.

Yang, P., Ai, L.-S., Huang, S.-C., Li, H.-F., Chan, W.-E., Chang, C.-W., Ko, C.-Y., & Chen, S. S.-L. (2010). The cytoplasmic domain of human immunodeficiency virus type 1 transmembrane protein gp41 harbors lipid raft association determinants. *Journal of Virology*, *84*(1), 59–75.

Zhu, T., Korber, B. T., Nahmias, A. J., Hooper, E., Sharp, P. M., & Ho, D. D. (1998). An African HIV-1 sequence from 1959 and implications for the origin of the epidemic. *Nature*, *391*(6667), 594–7.